

UNIVERSITÄT LEIPZIG
FAKULTÄT FÜR MATHEMATIK UND INFORMATIK
MATHEMATISCHES INSTITUT

Multimodal image registration by elastic matching
of edge sketches via optimal control

Angel Angelov and Marcus Wagner

Preprint-Reihe des Mathematischen Instituts

Preprint Nr. 04/2012

Multimodal image registration by elastic matching of edge sketches via optimal control

*Angel Angelov and Marcus Wagner**

Abstract. For the problem of multimodal image registration, an optimal control approach is presented. The geometrical information of the images will be transformed into weighted edge sketches, for which a linear-elastic or hyperelastic registration will be performed. For the numerical solution of this problem, we provide a direct method based on discretization methods and large-scale optimization techniques. A comparison of a separated and a joint access for the generation of the edge sketches and the determination of the matching deformation is made. The quality of the results obtained with the optimal control method competes well with those generated by a standard variational method.

1. Introduction.

Among the most challenging tasks of mathematical image processing is the registration of images with different modalities. In many application areas, e. g. medical tomography, astrophysics and geology, certain objects are imaged by different devices, at different wavelengths and by use of different imaging protocols.⁰¹⁾ In medical imaging, an analogous situation arises when contrasting agents or markers are applied, leading to intermittent changes of the modality even of images subsequently generated by a single device (compare Figs. 1 and 3 below). In all these cases, the question arises how to bring the different data sets into spatial correspondence.

In the mathematical formulation of this problem, two greyscale images are given, which will be modeled as functions $I(s), J(s): \Omega \rightarrow [0, 1]$ on a rectangular domain $\Omega \subset \mathbb{R}^2$.⁰²⁾ I is considered as reference image. If both images have the same modality, i. e. if the greyscale intensity scales in I and J are closely related then we may search for a deformation field $Z(s): \Omega \rightarrow \mathbb{R}^2$ fulfilling the condition $J(s - Z(s)) \approx I(s)$, thus modifying the template J such that it matches the reference image I in a best possible way.⁰³⁾ In multimodal matching, however, we cannot expect from the outset that the intensity scales in I and J correspond in a definite way. Consequently, the information contained in both images must be transformed into a quantity, which allows for a subsequent comparison. Now the condition to be fulfilled is $\mathcal{F}'(J(s - Z(s))) \approx \mathcal{F}''(I(s))$ where \mathcal{F}' , \mathcal{F}'' denote appropriate transformations of the image data.

Depending on the particular situation, different transformations of multimodal data have been proposed in the literature. Most frequently, the registration will be based on statistical quantities like correlation or mutual information, cf. [HERMOSILLO/CHEFD'HOTEL/FAUGERAS 02], pp. 332 ff., and [MODERSITZKI 09], pp. 97 ff., or on the geometrical information contained in the images (comparison of gradient or curvature properties), cf. [DROSKE/RUMPF 04], [DROSKE/RUMPF 07], [FISCHER/MODERSITZKI 03], [HABER/MODERSITZKI 07] and [MODERSITZKI 09], p. 331 f. For example, considering the definition

$$g_\sigma(I(s)) = \nabla I(s) / \sqrt{\|\nabla I(s)\|^2 + \sigma^2} \tag{1.1}$$

* Corresponding author.

⁰¹⁾ For example, [GALLARDO/MEJU 05] addresses the matching of electrical resistivity and seismic velocity data in order to draw conclusions about flow and transport processes in rocky near-surface materials.

⁰²⁾ In the following, we confine ourselves to the registration of two-dimensional data. The approach presented in this paper, however, works in higher dimensions as well.

⁰³⁾ [MODERSITZKI 09] and [ZITOVÁ/FLUSSER 03] provide general surveys of image registration methods.

of the normalized gradient field of a given image $I(s) \in C^1(\Omega, \mathbb{R})$ (cf. [HABER/MODERSITZKI 07], p. 295) where $\sigma > 0$ is sufficiently small, the deformation $Z(s)$ can be determined in such a way that the distance functional

$$\int_{\Omega} \left(1 - \left(g_{\sigma}(J(s - Z(s)))^T g_{\sigma}(I(s)) \right)^2 \right) ds \quad (1.2)$$

will be minimized, cf. [MODERSITZKI 09], p. 107 f.

In the present paper, we pursue the second way but present a slightly different approach of exploiting the geometrical properties of the images. Instead of normalized gradient fields, we generate *weighted edge sketches* $S_I, S_J: \Omega \rightarrow [0, 1]$ of I and J (as shown e. g. in Figs. 4 and 6) and attribute the differences between them to an *elastic deformation* Z of the pictured objects.⁰⁴⁾ Consequently, Z must satisfy the condition $S_J(s - Z(s)) \approx S_I(s)$. Since human tissue behaves according to hyperelastic material laws (see e. g. [OGDEN 03]), the proposed approach is particularly reasonable in medical imaging. Like other problems in mathematical imaging, the resulting elastic registration problem allows for an effective solution within the framework of multidimensional control within Sobolev spaces.⁰⁵⁾ In this problem, the objective

$$F(Z; S_J, S_I, \mu) = \int_{\Omega} (S_J(s - Z(s)) - S_I(s))^2 ds + \mu \int_{\Omega} r(\text{Jac } Z(s)) ds \quad (1.3)$$

consists of a fidelity term for the minimization of the grey value difference $(S_J(s - Z(s)) - S_I(s))^2$ of the weighted edge sketches and a regularization term,⁰⁶⁾ which corresponds to a particular elasticity model via the Euler-Lagrange equations of the problem. Since the validity of the underlying elasticity models can be guaranteed only as far as the shear stress generated by the deformation Z remains below a certain bound, a gradient restriction for the unknown deformation must be incorporated into the statement of the problem. Following [FRANEK/FRANEK/MAURER/WAGNER 12], pp. 287 ff., the edge sketches S_J and S_I can be obtained from a solution of a multidimensional control problem of analogous type as well.

First, we study the *separated access* where the three arising control problems for edge detection and matching of the edge sketches are subsequently solved. Then we investigate a *joint control problem*, which searches for the edge sketches and a matching deformation between them simultaneously. Selected numerical results of both accesses are presented. The registration quality will be quantified and evaluated by different indicators, e. g. by the relative reconstruction error for the edge sketches. Although the results of multimodal matching do not reach the reconstruction quality of comparable unimodal registration experiments (cf. [WAGNER 12], pp. 497 ff.), the output of the optimal control method competes well with those of the state-of-art variational method FAIR, which has been chosen as a reference.⁰⁷⁾ The computations have been carried out within the framework of the diploma thesis [ANGELOV 11] of the first author.

The plan of the investigation is as follows: In *Section 2*, we present an optimal control approach to the edge detection as well as to the elastic image registration problem. In the latter, the underlying elasticity models have been chosen in a representative way for describing linear-elastic and hyperelastic deformations, respectively, but we neither made adaptations to a particular material nor specified material parameters. In

⁰⁴⁾ In the literature, elastic registration is documented to be among the most popular methods in unimodal image matching. More details may be found in [HINTERMÜLLER/KEELING 09] and [MODERSITZKI 04], pp. 83 ff. The majority of approaches relies on linear elasticity, but recently there is a growing interest in hyperelastic models, cf. [BURGER/MODERSITZKI/RUTHOTTO 13], [WAGNER 10] and [WAGNER 12].

⁰⁵⁾ As documented in [WAGNER 10] and [WAGNER 12].

⁰⁶⁾ Cf. [SCHERZER/GRASMAIR/GROSSAUER/HALTMEIER/LENZEN 09] for regularization methods in image processing.

⁰⁷⁾ FAIR has been documented in [MODERSITZKI 09], pp. 9 ff., the software being distributed together with the textbook.

Section 3, we formulate a further control problem for joint determination of the edge sketches S_I , S_J and the elastic deformation Z and discuss the relation between its solutions and those of the separate problems from *Section 2*. *Section 4* is concerned with a common discretization scheme for the problems and its numerical solution. In *Section 5*, we describe first how to visualize the solutions and discuss different criteria for their quantitative evaluation. Then the test images used in the numerical experiments are documented. Finally, selected results of numerical experiments for the separated as well as for the joint access will be presented and discussed.

Notations.

Let $\Omega \subset \mathbb{R}^m$ be the closure of a bounded Lipschitz domain (in strong sense). Then $L^p(\Omega, \mathbb{R}^r)$ denotes the space of r -dimensional vector functions $f: \Omega \rightarrow \mathbb{R}^r$, whose components are integrable in the p th power ($1 \leq p < \infty$) or are measurable and essentially bounded ($p = \infty$). Further, $W_0^{1,p}(\Omega, \mathbb{R}^r)$ denotes the Sobolev space of r -dimensional vector functions $f: \Omega \rightarrow \mathbb{R}^r$ with compactly supported components, possessing first-order weak partial derivatives and belonging together with them to the space $L^p(\Omega, \mathbb{R})$ ($1 \leq p < \infty$). $W_0^{1,\infty}(\Omega, \mathbb{R}^r)$ is understood as the Sobolev space of all r -vector functions $f: \Omega \rightarrow \mathbb{R}^r$ with Lipschitz continuous components and boundary values zero, cf. [EVANS/GARIEPY 92], p. 131, Theorem 5. $Jac Z$ denotes the Jacobian matrix of the vector function $Z \in W_0^{1,p}(\Omega, \mathbb{R}^r)$. The symbol \mathbf{o} denotes, depending on the context, the zero element or the zero function of the underlying space. Finally, the abbreviation “ $(\forall) s \in A$ ” has to be read as “for almost all $s \in A$ ” or “for all $s \in A$ except a Lebesgue null set”.

2. Separate search for the edge sketches and the matching deformation.

a) Edge detection by optimal control.

The geometrical information contained in a pair (I, J) of template and reference image with different modalities will be extracted by generating a pair of weighted edge sketches S_I, S_J . Following [FRANEK/FRANEK/MAURER/WAGNER 12], this can be done by solving the multidimensional control problems

$$(E)_1 \quad F_{edge}(X; I, \lambda) = \int_{\Omega} (X(s) - I(s))^2 ds + \lambda \int_{\Omega} \left(\left(\frac{\partial X}{\partial s_1}(s) \right)^2 + \left(\frac{\partial X}{\partial s_2}(s) \right)^2 + \delta^2 \right)^{1/2} ds \longrightarrow \inf!; \quad (2.1)$$

$$X \in W_0^{1,p}(\Omega, \mathbb{R}); \quad |\nabla X(s)|^2 \leq R^2 \quad (\forall) s \in \Omega \quad \text{and} \quad (2.2)$$

$$(E)_2 \quad F_{edge}(Y; J, \lambda) = \int_{\Omega} (Y(s) - J(s))^2 ds + \lambda \int_{\Omega} \left(\left(\frac{\partial Y}{\partial s_1}(s) \right)^2 + \left(\frac{\partial Y}{\partial s_2}(s) \right)^2 + \delta^2 \right)^{1/2} ds \longrightarrow \inf!; \quad (2.3)$$

$$Y \in W_0^{1,p}(\Omega, \mathbb{R}); \quad |\nabla Y(s)|^2 \leq R^2 \quad (\forall) s \in \Omega, \quad (2.4)$$

which result in denoising/smoothing of the original image data while allowing for simultaneous edge detection: we interpret those subsets of Ω as edges where the gradient restrictions (2.2) or (2.4) become nearly active. In $(E)_1$ and $(E)_2$, we use $p \geq 1$, $\delta > 0$, a regularization parameter $\lambda > 0$ and a further parameter $R > 0$ providing a restriction for the intensity gradients in the denoised versions X and Y of I and J . For sufficiently small values $\delta > 0$, the anisotropic regularization term $\int_{\Omega} \sqrt{|\nabla X|^2 + \delta^2} ds$ may be understood as an approximation for the total variation norm of ∇X avoiding its main disadvantages⁰⁸⁾ while conserving quite fairly the edge structure within the image. Given optimal solutions \hat{X} and \hat{Y} of $(E)_1$ and $(E)_2$, we interpret

⁰⁸⁾ In this approximation, the integrand is differentiable at \mathbf{o} and produces only reduced staircasing.

as “edges” those subsets of Ω where the gradient restrictions (2.2) and (2.4) become nearly active. Thus the edge sketches $S_{\hat{X}}, S_{\hat{Y}} \in L^\infty(\Omega, \mathbb{R})$ will be obtained through

$$S_{\hat{X}}(s) = 1 - \frac{1}{R^2} \left(|\nabla \hat{X}(s)|^2 + \varepsilon^2 \right)^{1/n}; \quad (2.5)$$

$$S_{\hat{Y}}(s) = 1 - \frac{1}{R^2} \left(|\nabla \hat{Y}(s)|^2 + \varepsilon^2 \right)^{1/n} \quad (2.6)$$

with $\varepsilon > 0$ and $n \in \mathbb{N}$, $n \geq 2$. Since enlargement of n results in a moderate fill-in effect for the edge sketches, we used $n = 4$ in most of the subsequent experiments.⁰⁹⁾ As the following theorem states, the existence of minimizers in (E)₁ and (E)₂ can be ensured.

Theorem 2.1.¹⁰⁾ *Under the assumptions mentioned above, the problems (E)₁ and (E)₂ admit global minimizers $\hat{X}, \hat{Y} \in W_0^{1,\infty}(\Omega, \mathbb{R})$.*

b) Elastic/hyperelastic image registration by optimal control.

The next step is the unimodal registration of the edge sketches $S_{\hat{X}}$ and $S_{\hat{Y}}$. As shown in [WAGNER 10] and [WAGNER 12], this problem allows for an optimal control formulation as well. Let us consider the problem

$$(R) \quad F(Z; S_{\hat{Y}}, S_{\hat{X}}, \mu) = \int_{\Omega} (S_{\hat{Y}}(s - Z(s)) - S_{\hat{X}}(s))^2 ds + \mu \int_{\Omega} r(\text{Jac } Z(s)) ds \longrightarrow \inf!; \quad (2.7)$$

$$Z \in W_0^{1,p}(\Omega, \mathbb{R}^2); \quad \text{Jac } Z(s) \in \mathbf{K} \quad (\forall) s \in \Omega \quad (2.8)$$

with $p \geq 1$. Here Z denotes the unknown elastic deformation, $\mu > 0$ is the regularization parameter, the convex or polyconvex function $r(v): \mathbb{R}^{2 \times 2} \rightarrow \mathbb{R}$ (cf. [DACOROGNA 08], p. 156 f., Definition 5.1., (iii)) specifies the underlying elasticity model, and $\mathbf{K} \subset \mathbb{R}^{2 \times 2}$ is a convex, compact set with $\mathbf{o} \in \text{int}(\mathbf{K})$. The introduction of the gradient constraint (2.8) reflects the fact that the validity of any underlying elasticity model can be ensured only while the shear stress generated by the deformation Z , which is proportional to $\|JZ\|$, remains uniformly bounded. In particular, for a linear-elastic registration we choose the convex integrand

$$r\left(\begin{smallmatrix} a & b \\ c & d \end{smallmatrix}\right) = 4a^2 + 2(b+c)^2 + 4d^2, \quad (2.9)$$

cf. [HENN/WITSCH 01], p. 1079 f., and for a hyperelastic registration the polyconvex integrand

$$r\left(\begin{smallmatrix} a & b \\ c & d \end{smallmatrix}\right) = \gamma_1 \|E_2 - \begin{smallmatrix} a & b \\ c & d \end{smallmatrix}\|^p + \gamma_2 \text{Det}^2\left(E_2 - \begin{smallmatrix} a & b \\ c & d \end{smallmatrix}\right) \quad (2.10)$$

with positive weights $\gamma_1, \gamma_2 > 0$ and $p \geq 1$ while E_2 denotes the (2,2)-unit matrix.¹¹⁾ As discussed in [WAGNER 10] and [WAGNER 12], it is advisable to replace the fidelity term in (2.7) by a second-order Taylor expansion with third-order remainder term, and to replace further the (formal) derivatives of $S_{\hat{Y}}$ within this expansion by appropriate finite-difference approximations $\nabla S_{\hat{Y}} \approx DS_{\hat{Y}} \in L^\infty(\Omega, \mathbb{R}^2)$ and $\nabla^2 S_{\hat{Y}} \approx D^2 S_{\hat{Y}} \in L^\infty(\Omega, \mathbb{R}^{2 \times 2})$, see (4.1) – (4.5) below. As a result, we obtain the following approximation for the integrand within the fidelity term in (2.7):

$$S_{\hat{Y}}(s - Z(s)) - S_{\hat{X}}(s) \approx S_{\hat{Y}}(s) - DS_{\hat{Y}}(s)^T Z(s) + \frac{1}{2} Z(s)^T D^2 S_{\hat{Y}}(s) Z(s) + \frac{1}{6} G(s) \cdot \|Z(s)\|^3 - S_{\hat{X}}(s). \quad (2.11)$$

⁰⁹⁾ In the following, exceptions are explicitly mentioned.

¹⁰⁾ [FRANEK/FRANEK/MAURER/WAGNER 12], p. 280, Theorem 2.1., together with p. 289.

¹¹⁾ This regularization is related to a generic hyperelastic material law, cf. [DROSKE/RUMPF 04], p. 673.

When inserting an admissible state $Z \in W_0^{1,\infty}(\Omega, \mathbb{R}^2)$ into (2.11), we may identify $G(\cdot)$ as a measurable, essentially bounded function. As long as G remains sufficiently small, which will be ensured by considering an additional state constraint $|G(s)| \leq \eta_{max}$, the character of Z as an elastic deformation will be preserved. G may be interpreted as a small grey value correction, to be applied to the reconstructed edge sketch.

c) Final statement of the registration problem.

Summing up, we arrive at the following multidimensional control problems:

$$(R)_{lin} \quad F_{lin}(Z, G; S_{\hat{Y}}, S_{\hat{X}}, \mu) \tag{2.12}$$

$$= \int_{\Omega} \left(S_{\hat{Y}}(s) - DS_{\hat{Y}}(s)^T Z(s) + \frac{1}{2} Z(s)^T D^2 S_{\hat{Y}}(s) Z(s) + \frac{1}{6} G(s) \cdot \|Z(s)\|^3 - S_{\hat{X}}(s) \right)^2 ds \\ + \mu \int_{\Omega} \left(4 \left(\frac{\partial Z_1}{\partial s_1}(s) \right)^2 + 2 \left(\frac{\partial Z_1}{\partial s_2}(s) + \frac{\partial Z_2}{\partial s_1}(s) \right)^2 + 4 \left(\frac{\partial Z_2}{\partial s_2}(s) \right)^2 \right) ds \longrightarrow \inf!;$$

$$(Z, G) \in W_0^{1,p}(\Omega, \mathbb{R}^2) \times L^\infty(\Omega, \mathbb{R}); \tag{2.13}$$

$$|G(s)| \leq \eta_{max} \quad (\forall) s \in \Omega; \tag{2.14}$$

$$Jac Z(s) \in K = \left\{ \begin{pmatrix} a & b \\ c & d \end{pmatrix} \in \mathbb{R}^{2 \times 2} \mid a^2 + b^2 + c^2 + d^2 \leq T^2 \right\} \quad (\forall) s \in \Omega \tag{2.15}$$

(linear-elastic registration of edge sketches, unimodal) with $p \geq 1$, $\eta_{max} > 0$, a regularization parameter $\mu > 0$ and the control parameter $T > 0$ occurring in the description of the convex set $K \subset \mathbb{R}^{2 \times 2}$. Further, we state

$$(R)_{hyp} \quad F_{hyp}(Z, G; S_{\hat{Y}}, S_{\hat{X}}, \mu) \tag{2.16}$$

$$= \int_{\Omega} \left(S_{\hat{Y}}(s) - DS_{\hat{Y}}(s)^T Z(s) + \frac{1}{2} Z(s)^T D^2 S_{\hat{Y}}(s) Z(s) + \frac{1}{6} G(s) \cdot \|Z(s)\|^3 - S_{\hat{X}}(s) \right)^2 ds \\ + \mu \int_{\Omega} \left(\gamma_1 \|E_2 - Jac Z(s)\|^p + \gamma_2 Det^2(E_2 - Jac Z(s)) \right) ds \longrightarrow \inf!;$$

$$(Z, G) \in W_0^{1,p}(\Omega, \mathbb{R}^2) \times L^\infty(\Omega, \mathbb{R}); \tag{2.17}$$

$$|G(s)| \leq \eta_{max} \quad (\forall) s \in \Omega; \tag{2.18}$$

$$Jac Z(s) \in K = \left\{ \begin{pmatrix} a & b \\ c & d \end{pmatrix} \in \mathbb{R}^{2 \times 2} \mid a^2 + b^2 + c^2 + d^2 \leq T^2 \right\} \quad (\forall) s \in \Omega \tag{2.19}$$

(hyperelastic registration of edge sketches, unimodal) with $p \geq 1$, $\gamma_1, \gamma_2, \eta_{max} > 0$, a regularization parameter $\mu > 0$ and the control parameter $T > 0$. Again, the convex set K has been specified as a four-dimensional closed ball with radius T . For the convex problem $(R)_{lin}$ as well as for the polyconvex problem $(R)_{hyp}$, the existence of minimizers can be proven.

Theorem 2.2.¹²⁾ *Under the assumptions mentioned above, the problems $(R)_{lin}$ as well as $(R)_{hyp}$ admit global minimizers for any pair of edge sketches $\hat{X}, \hat{Y} \in L^\infty(\Omega, \mathbb{R}^2)$ and finite-difference approximations $DS_{\hat{Y}} \in L^\infty(\Omega, \mathbb{R}^2)$, $D^2 S_{\hat{Y}} \in L^\infty(\Omega, \mathbb{R}^{2 \times 2})$ for the derivatives of \hat{Y} .*

¹²⁾ [WAGNER 12], p. 492, Theorems 2.1. and 2.2.

3. Joint generation of the edge sketches and the matching deformation.

a) Statement of the joint problem.

Instead of obtaining a matching deformation as a result of the subsequent solution of three separate optimal control problems, we may combine the three tasks of determining S_X , S_Y and Z into a joint problem. As suggested in the literature, the objective in the joint problem arises as an appropriate linear combination of the objectives of the separate problems.¹³⁾ We obtain

$$\begin{aligned} (\mathbf{R})_{joint,lin} \quad & F_{joint,lin}(X, Y, Z, G) \\ & = \alpha F_{edge}(X; I, \lambda) + \alpha F_{edge}(Y; J, \lambda) + \beta F_{lin}(Z, G; S_Y, S_X, \mu) \longrightarrow \inf !; \end{aligned} \quad (3.1)$$

$$(X, Y, Z, G) \in W_0^{1,p}(\Omega, \mathbb{R}) \times W_0^{1,p}(\Omega, \mathbb{R}) \times W_0^{1,p}(\Omega, \mathbb{R}^2) \times L^\infty(\Omega, \mathbb{R}); \quad (3.2)$$

$$S_X(s) = 1 - \frac{1}{R^2} \left(|\nabla X(s)|^2 + \varepsilon^2 \right)^{1/n} \quad \forall s \in \Omega; \quad (3.3)$$

$$S_Y(s) = 1 - \frac{1}{R^2} \left(|\nabla Y(s)|^2 + \varepsilon^2 \right)^{1/n} \quad \forall s \in \Omega; \quad (3.4)$$

$$|\nabla X(s)|^2 \leq R^2, \quad |\nabla Y(s)|^2 \leq R^2, \quad |G(s)| \leq \eta_{max} \quad (\forall) s \in \Omega; \quad (3.5)$$

$$Jac Z(s) \in \mathbf{K} = \left\{ \begin{pmatrix} a & b \\ c & d \end{pmatrix} \in \mathbb{R}^{2 \times 2} \mid a^2 + b^2 + c^2 + d^2 \leq T^2 \right\} \quad (\forall) s \in \Omega \quad (3.6)$$

(linear-elastic registration, multimodal) with $p \geq 1$, $\alpha, \beta, \delta, \varepsilon, \eta_{max} > 0$, $n \in \{2, 4\}$, regularization parameters $\lambda, \mu > 0$ and control parameters $R, T > 0$, and

$$\begin{aligned} (\mathbf{R})_{joint,hyp} \quad & F_{joint,hyp}(X, Y, Z, G) \\ & = \alpha F_{edge}(X; I, \lambda) + \alpha F_{edge}(Y; J, \lambda) + \beta F_{hyp}(Z, G; S_Y, S_X, \mu) \longrightarrow \inf !; \end{aligned} \quad (3.7)$$

$$(X, Y, Z, G) \in W_0^{1,p}(\Omega, \mathbb{R}) \times W_0^{1,p}(\Omega, \mathbb{R}) \times W_0^{1,p}(\Omega, \mathbb{R}^2) \times L^\infty(\Omega, \mathbb{R}); \quad (3.8)$$

$$S_X(s) = 1 - \left(|\nabla X(s)|^2 / R^2 + \varepsilon^2 / R^2 \right)^{1/n} \quad \forall s \in \Omega; \quad (3.9)$$

$$S_Y(s) = 1 - \left(|\nabla Y(s)|^2 / R^2 + \varepsilon^2 / R^2 \right)^{1/n} \quad \forall s \in \Omega; \quad (3.10)$$

$$|\nabla X(s)|^2 \leq R^2, \quad |\nabla Y(s)|^2 \leq R^2, \quad |G(s)| \leq \eta_{max} \quad (\forall) s \in \Omega; \quad (3.11)$$

$$Jac Z(s) \in \mathbf{K} = \left\{ \begin{pmatrix} a & b \\ c & d \end{pmatrix} \in \mathbb{R}^{2 \times 2} \mid a^2 + b^2 + c^2 + d^2 \leq T^2 \right\} \quad (\forall) s \in \Omega \quad (3.12)$$

(hyperelastic registration, multimodal) with $p \geq 1$, $\alpha, \beta, \gamma_1, \gamma_2, \delta, \varepsilon, \eta_{max} > 0$, $n \in \{2, 4\}$, regularization parameters $\lambda, \mu > 0$ and control parameters $R, T > 0$. In both problems $(\mathbf{R})_{joint,lin}$ and $(\mathbf{R})_{joint,hyp}$, the convex set \mathbf{K} has been specified as a four-dimensional closed ball with radius T .

b) Comparison with the separated access.

Let us assume that minimal solutions \hat{X} , \hat{Y} and (\hat{Z}, \hat{G}) for the problems $(\mathbf{E})_1$, $(\mathbf{E})_2$ and $(\mathbf{R})_{lin}$ from the separated access are given where $(\mathbf{R})_{lin}$ has been solved for the edge sketches $S_{\hat{Y}}$ and $S_{\hat{X}}$ generated from \hat{Y}

¹³⁾ Similar approaches have been proposed for a number of image processing problems. To mention only a few examples related to the problems studied in the present paper, we refer to [BOURDIN 99], p. 232, (7), [DROSKE/RUMPF 07] and [HAN ET AL. 06], p. 247.

and \hat{X} . The corresponding minimal values are denoted by m_1 , m_2 and m_3 . Then, keeping the parameters p , δ , ε , η_{max} , n , λ , μ , R and T and inserting them into $(R)_{joint,lin}$, we observe that $(\hat{X}, \hat{Y}, \hat{Z}, \hat{G})$ forms a feasible solution for this problem. Consequently, the minimal value m of $(R)_{joint,lin}$ satisfies

$$F_{joint,lin}(\hat{X}, \hat{Y}, \hat{Z}, \hat{G}) = \alpha(m_1 + m_2) + \beta m_3 \geq m. \quad (3.13)$$

In complete analogy, we observe that a quadruple of minimal solutions \hat{X} , \hat{Y} and (\hat{Z}, \hat{G}) for the problems $(E)_1$, $(E)_2$ and $(R)_{hyp}$ forms a feasible solution for $(R)_{joint,hyp}$ as far as the corresponding parameters have been transferred. Consequently, we may expect that the joint access is able to refine the results obtained from the separated strategy. The price to pay is that we must deal with a much larger problem involving a nonlinear coupling of the unknown variables, namely (3.3), (3.4), (3.9) and (3.10). In fact, we cannot even guarantee the existence of global minimizers in $(R)_{joint,lin}$ or $(R)_{joint,hyp}$ due to the incompatibility of (3.3), (3.4), (3.9) and (3.10) with the weak*-convergence of subsequences $\{\nabla X^N\}$ and $\{\nabla Y^N\}$ derived from a minimizing sequence. In our numerical experiments, however, an appropriate choice of the global weights α and β in (3.1) and (3.7) turned out to be $\alpha = 6000$ and $\beta = 1$; thus the image representations \tilde{X} , \tilde{Y} and the edge sketches $S_{\tilde{X}}$, $S_{\tilde{Y}}$ obtained from an approximate solution of $(R)_{joint,lin}$ or $(R)_{joint,hyp}$ can be considered as nearly optimal in $(E)_1$ and $(E)_2$.

4. Numerical solution by direct methods.

a) The discretization strategy.

For the numerical solution of the multidimensional control problems $(E)_1$, $(E)_2$, $(R)_{lin}$, $(R)_{hyp}$, $(R)_{joint,lin}$ and $(R)_{joint,hyp}$ from Sections 2 and 3, we pursue the strategy “first discretize, then optimize”. Within the square domain $\Omega = [0, K] \times [0, L]$ with $K = L = 2^N$, we generate a regular triangulation (cf. [GOERING/ROOS/TOBISKA 93], pp. 28 and 40, (Z1) – (Z4), and p. 138, (Z5)), introducing first a grid of squares $Q_{k,l} = \square(s_{k-1,l-1}, s_{k,l-1}, s_{k,l}, s_{k-1,l})$, $1 \leq k \leq K$, $1 \leq l \leq L$, with edge length 1 and then splitting every square along the principal diagonal into two triangles $\Delta'_{k,l} = \Delta(s_{k-1,l-1}, s_{k,l-1}, s_{k,l})$ and $\Delta''_{k,l} = \Delta(s_{k-1,l-1}, s_{k,l}, s_{k-1,l})$, thus getting discretized problems $(E)_1^N, \dots$, accordingly.

The necessary optimality conditions for the discretized problems take the form of large-scale systems of nonlinear equations, for those solution an interior-point method has been employed, cf. [JANSEN 97]. As the input/output platform for the image data, MATLAB has been used; the discretized problems have been programmed with the help of the modelling language AMPL (cf. [FOURER/GAY/KERNIGHAN 03]) and then transferred to the interior-point solver IPOPT.¹⁴⁾ The results have been represented and evaluated with MATLAB again.

b) The access with three separate problems.

For the discretization of the problems $(E)_1$, $(E)_2$ and $(R)_{lin}$, $(R)_{hyp}$, we refer to [FRANEK/FRANEK/MAURER/WAGNER 12], p. 289 f., and [WAGNER 12], p. 493 f. Note that in all problems, in order to cope with the possible discontinuity of the generalized partial derivatives belonging to L^∞ instead of C^0 , the number of the corresponding discretization variables must be doubled. On $Q_{k,l}$, $2 \leq k \leq K - 2$, $2 \leq l \leq L - 2$, the finite-difference approximations for the partial derivatives of $S_{\hat{Y}}$ in (2.11) read as follows:

$$\frac{\partial S_{\hat{Y}}}{\partial s_1}(s) \approx D_{s_1} S_{\hat{Y}}(s_{k,l}) = \frac{1}{9} \cdot \sum_{i,j=-1}^1 \left(\frac{1}{2} (S_{\hat{Y}}(s_{k+1+i,l+j}) - S_{\hat{Y}}(s_{k-1+i,l+j})) \right); \quad (4.1)$$

$$\frac{\partial S_{\hat{Y}}}{\partial s_2}(s) \approx D_{s_2} S_{\hat{Y}}(s_{k,l}) = \frac{1}{9} \cdot \sum_{i,j=-1}^1 \left(\frac{1}{2} (S_{\hat{Y}}(s_{k+i,l+1+j}) - S_{\hat{Y}}(s_{k+i,l-1+j})) \right); \quad (4.2)$$

¹⁴⁾ Cf. [LAIRD/WÄCHTER 09] and [WÄCHTER/BIEGLER 06]. The experiments have been performed with version 3.8.

$$\frac{\partial^2 S_{\hat{Y}}}{(\partial s_1)^2}(s) \approx D_{s_1 s_1}^2 S_{\hat{Y}}(s_{k,l}) = \frac{1}{9} \cdot \sum_{i,j=-1}^1 \left(\frac{1}{2} (S_{\hat{Y}}(s_{k+1+i,l+j}) - 2S_{\hat{Y}}(s_{k+i,l+j}) + S_{\hat{Y}}(s_{k-1+i,l+j})) \right); \quad (4.3)$$

$$\begin{aligned} \frac{\partial^2 S_{\hat{Y}}}{\partial s_1 \partial s_2}(s) \approx D_{s_1 s_2}^2 S_{\hat{Y}}(s_{k,l}) &= \frac{1}{9} \cdot \sum_{i,j=-1}^1 \left(\frac{1}{4} (S_{\hat{Y}}(s_{k+1+i,l+1+j}) \right. \\ &\quad \left. - S_{\hat{Y}}(s_{k-1+i,l+1+j}) - S_{\hat{Y}}(s_{k+1+i,l-1+j}) + S_{\hat{Y}}(s_{k-1+i,l-1+j})) \right); \end{aligned} \quad (4.4)$$

$$\frac{\partial^2 S_{\hat{Y}}}{(\partial s_2)^2}(s) \approx D_{s_2 s_2}^2 S_{\hat{Y}}(s_{k,l}) = \frac{1}{9} \cdot \sum_{i,j=-1}^1 \left(\frac{1}{2} (S_{\hat{Y}}(s_{k+i,l+1+j}) - 2S_{\hat{Y}}(s_{k+i,l+j}) + S_{\hat{Y}}(s_{k+i,l-1+j})) \right), \quad (4.5)$$

cf. [WAGNER 12], p. 490, Subsection 2.b). In order to find appropriate values for the regularization parameters $\lambda, \mu > 0$ and the control parameters $R, T > 0$, based on the range indications from [FRANEK/FRANEK/MAURER/WAGNER 12] and [WAGNER 12], a number of additional experiments has been made.

In the numerical solution of the discretized problems (E)₁^N and (E)₂^N, we observed that the final solution is approached by IPOPT remarkably fast. Consequently, we must perform only a few iteration steps in order to get the desired edge sketches.¹⁵⁾

c) Remarks about the solution of the joint problem.

For the joint problem (R)_{joint,lin}, we will provide the complete formulation of the corresponding discretized problem (R)_{joint,lin}^N. In the following, X corresponds with the discretization variables $x_{k,l}$, ∇X with $\begin{pmatrix} v_{(2,1)}^{(1,1)} \\ v_{(2,2)}^{(1,2)} \end{pmatrix}$, Y with $y_{k,l}$, ∇Y with $\begin{pmatrix} w_{(2,1)}^{(1,1)} \\ w_{(2,2)}^{(1,2)} \end{pmatrix}$, S_X with $\sigma_{k,l}^{(x)}$, S_Y with $\sigma_{k,l}^{(y)}$, Z with $z_{k,l}^{(1)}$ and $z_{k,l}^{(2)}$, $Jac Z$ with $\begin{pmatrix} \zeta_{(2,1,1)}^{(1,1,1)} & \zeta_{(2,2,1)}^{(1,2,1)} \\ \zeta_{(2,1,2)}^{(1,1,2)} & \zeta_{(2,2,2)}^{(1,2,2)} \end{pmatrix}$, and G with $\eta_{k,l}$.

$$\begin{aligned} (R)_{joint,lin}^N \tilde{F}_{joint,lin} &\left(x_{0,0}, \dots, x_{K,L}, v_{1,1}^{(1,1)}, \dots, v_{K,L}^{(2,2)}, y_{0,0}, \dots, y_{K,L}, w_{1,1}^{(1,1)}, \dots, w_{K,L}^{(2,2)} \right. \\ &\quad \left. z_{0,0}^{(1)}, \dots, z_{K,L}^{(2)}, \zeta_{1,1}^{(1,1,1)}, \dots, \zeta_{K,L}^{(2,2,2)}, \eta_{0,0}, \dots, \eta_{K,L}, \sigma_{1,1}^{(x)}, \dots, \sigma_{K,L}^{(x)}, \sigma_{1,1}^{(y)}, \dots, \sigma_{K,L}^{(y)} \right) \\ &= \alpha \tilde{F}_{edge} \left(x_{0,0}, \dots, x_{K,L}, v_{1,1}^{(1,1)}, \dots, v_{K,L}^{(2,2)} \right) + \alpha \tilde{F}_{edge} \left(y_{0,0}, \dots, y_{K,L}, w_{1,1}^{(1,1)}, \dots, w_{K,L}^{(2,2)} \right) \\ &\quad + \beta \tilde{F}_{lin} \left(z_{0,0}^{(1)}, \dots, z_{K,L}^{(2)}, \zeta_{1,1}^{(1,1,1)}, \dots, \zeta_{K,L}^{(2,2,2)}, \eta_{0,0}, \dots, \eta_{K,L}, \sigma_{1,1}^{(x)}, \dots, \sigma_{K,L}^{(x)}, \sigma_{1,1}^{(y)}, \dots, \sigma_{K,L}^{(y)} \right) \rightarrow \text{Min!}; \end{aligned} \quad (4.6)$$

$$\left(x_{0,0}, \dots, v_{K,L}^{(2,2)} \right) \times \left(y_{0,0}, \dots, w_{K,L}^{(2,2)} \right) \times \left(z_{0,0}^{(1)}, \dots, z_{K,L}^{(2)}, \zeta_{1,1}^{(1,1,1)}, \dots, \zeta_{K,L}^{(2,2,2)}, \right. \quad (4.7)$$

$$\left. \eta_{0,0}, \dots, \eta_{K,L} \right) \in \left(\mathbb{R}^{(K+1)(L+1)} \times \mathbb{R}^{4KL} \right)^2 \times \left(\mathbb{R}^{3(K+1)(L+1)} \times \mathbb{R}^{8KL} \right);$$

$$x_{0,l} = x_{K,l} = 0, \quad x_{k,0} = x_{k,L} = 0, \quad 0 \leq k \leq K, \quad 0 \leq l \leq L; \quad (4.8)$$

$$y_{0,l} = y_{K,l} = 0, \quad y_{k,0} = y_{k,L} = 0, \quad 0 \leq k \leq K, \quad 0 \leq l \leq L; \quad (4.9)$$

$$z_{0,l}^{(i)} = z_{K,l}^{(i)} = 0, \quad z_{k,0}^{(i)} = z_{k,L}^{(i)} = 0, \quad i = 1, 2, \quad 0 \leq k \leq K, \quad 0 \leq l \leq L; \quad (4.10)$$

$$\begin{pmatrix} v_{k,l}^{(1,1)} \\ v_{k,l}^{(2,1)} \end{pmatrix} = \begin{pmatrix} x_{k,l-1} - x_{k-1,l-1} \\ x_{k,l} - x_{k,l-1} \end{pmatrix}, \quad \begin{pmatrix} v_{k,l}^{(1,2)} \\ v_{k,l}^{(2,2)} \end{pmatrix} = \begin{pmatrix} x_{k,l} - x_{k-1,l} \\ x_{k-1,l} - x_{k-1,l-1} \end{pmatrix}, \quad 1 \leq k \leq K, \quad 1 \leq l \leq L; \quad (4.11)$$

$$\begin{pmatrix} w_{k,l}^{(1,1)} \\ w_{k,l}^{(2,1)} \end{pmatrix} = \begin{pmatrix} y_{k,l-1} - y_{k-1,l-1} \\ y_{k,l} - y_{k,l-1} \end{pmatrix}, \quad \begin{pmatrix} w_{k,l}^{(1,2)} \\ w_{k,l}^{(2,2)} \end{pmatrix} = \begin{pmatrix} y_{k,l} - y_{k-1,l} \\ y_{k-1,l} - y_{k-1,l-1} \end{pmatrix}, \quad 1 \leq k \leq K, \quad 1 \leq l \leq L; \quad (4.12)$$

$$\begin{pmatrix} \zeta_{k,l}^{(1,1,1)} & \zeta_{k,l}^{(1,2,1)} \\ \zeta_{k,l}^{(2,1,1)} & \zeta_{k,l}^{(2,2,1)} \end{pmatrix} = \begin{pmatrix} z_{k,l-1}^{(1)} - z_{k-1,l-1}^{(1)} & z_{k,l}^{(1)} - z_{k,l-1}^{(1)} \\ z_{k,l-1}^{(2)} - z_{k-1,l-1}^{(2)} & z_{k,l}^{(2)} - z_{k,l-1}^{(2)} \end{pmatrix}, \quad 1 \leq k \leq K, \quad 1 \leq l \leq L; \quad (4.13)$$

¹⁵⁾ Typically less than 10 iterations, cf. [ANGELOV 11], p. 74.

$$\begin{pmatrix} \zeta_{k,l}^{(1,1,2)} & \zeta_{k,l}^{(1,2,2)} \\ \zeta_{k,l}^{(2,1,2)} & \zeta_{k,l}^{(2,2,2)} \end{pmatrix} = \begin{pmatrix} z_{k,l}^{(1)} - z_{k-1,l}^{(1)} & z_{k-1,l}^{(1)} - z_{k-1,l-1}^{(1)} \\ z_{k,l}^{(2)} - z_{k-1,l}^{(2)} & z_{k-1,l}^{(2)} - z_{k-1,l-1}^{(2)} \end{pmatrix}, \quad 1 \leq k \leq K, \quad 1 \leq l \leq L; \quad (4.14)$$

$$\sigma_{k,l}^{(x)} = 1 - \frac{1}{R^2} \left(\frac{1}{2} (v_{k,l}^{(1,1)})^2 + \frac{1}{2} (v_{k,l}^{(2,1)})^2 + \frac{1}{2} (v_{k,l}^{(1,2)})^2 + \frac{1}{2} (v_{k,l}^{(2,2)})^2 \right)^{1/n}, \quad 1 \leq k \leq K, \quad 1 \leq l \leq L; \quad (4.15)$$

$$\sigma_{k,l}^{(y)} = 1 - \frac{1}{R^2} \left(\frac{1}{2} (w_{k,l}^{(1,1)})^2 + \frac{1}{2} (w_{k,l}^{(2,1)})^2 + \frac{1}{2} (w_{k,l}^{(1,2)})^2 + \frac{1}{2} (w_{k,l}^{(2,2)})^2 \right)^{1/n}, \quad 1 \leq k \leq K, \quad 1 \leq l \leq L; \quad (4.16)$$

$$|\eta_{k,l}| \leq \eta_{max}, \quad 0 \leq k \leq K, \quad 0 \leq l \leq L; \quad (4.17)$$

$$(v_{k,l}^{(1,1)})^2 + (v_{k,l}^{(2,1)})^2 \leq R^2, \quad (v_{k,l}^{(1,2)})^2 + (v_{k,l}^{(2,2)})^2 \leq R^2, \quad 1 \leq k \leq K, \quad 1 \leq l \leq L; \quad (4.18)$$

$$(w_{k,l}^{(1,1)})^2 + (w_{k,l}^{(2,1)})^2 \leq R^2, \quad (w_{k,l}^{(1,2)})^2 + (w_{k,l}^{(2,2)})^2 \leq R^2, \quad 1 \leq k \leq K, \quad 1 \leq l \leq L; \quad (4.19)$$

$$(\zeta_{k,l}^{(1,1,1)})^2 + (\zeta_{k,l}^{(1,2,1)})^2 + (\zeta_{k,l}^{(2,1,1)})^2 + (\zeta_{k,l}^{(2,2,1)})^2 \leq T^2, \quad 1 \leq k \leq K, \quad 1 \leq l \leq L; \quad (4.20)$$

$$(\zeta_{k,l}^{(1,1,2)})^2 + (\zeta_{k,l}^{(1,2,2)})^2 + (\zeta_{k,l}^{(2,1,2)})^2 + (\zeta_{k,l}^{(2,2,2)})^2 \leq T^2, \quad 1 \leq k \leq K, \quad 1 \leq l \leq L. \quad (4.21)$$

The discretized functionals $\tilde{F}_{edge}(\dots)$ read as follows:

$$\begin{aligned} \tilde{F}_{edge}(x_{0,0}, \dots, x_{K,L}, v_{1,1}^{(1,1)}, \dots, v_{K,L}^{(2,2)}) &= \frac{1}{2} \cdot \sum_{k=1}^K \sum_{l=1}^L \left((x_{k-1,l-1} - I(s_{k,l}))^2 + (x_{k,l} - I(s_{k,l}))^2 \right. \\ &\quad \left. + \lambda \sqrt{(v_{k,l}^{(1,1)})^2 + (v_{k,l}^{(2,1)})^2 + \delta^2} + \lambda \sqrt{(v_{k,l}^{(1,2)})^2 + (v_{k,l}^{(2,2)})^2 + \delta^2} \right); \end{aligned} \quad (4.22)$$

$$\begin{aligned} \tilde{F}_{edge}(y_{0,0}, \dots, y_{K,L}, w_{1,1}^{(1,1)}, \dots, w_{K,L}^{(2,2)}) &= \frac{1}{2} \cdot \sum_{k=1}^K \sum_{l=1}^L \left((y_{k-1,l-1} - J(s_{k,l}))^2 + (y_{k,l} - J(s_{k,l}))^2 \right. \\ &\quad \left. + \lambda \sqrt{(w_{k,l}^{(1,1)})^2 + (w_{k,l}^{(2,1)})^2 + \delta^2} + \lambda \sqrt{(w_{k,l}^{(1,2)})^2 + (w_{k,l}^{(2,2)})^2 + \delta^2} \right). \end{aligned} \quad (4.23)$$

Denoting the integrand within $F_{lin}(Z, G; S_Y, S_X, \mu)$ by $\varphi\left(\begin{pmatrix} Z^{(1)} \\ Z^{(2)} \end{pmatrix}, \begin{pmatrix} Z_{s_1}^{(1)} & Z_{s_2}^{(1)} \\ Z_{s_1}^{(2)} & Z_{s_2}^{(2)} \end{pmatrix}, G, S_Y, DS_Y, D^2S_Y, S_X\right)$, the discretized functional $\tilde{F}_{lin}(\dots)$ can be written as

$$\begin{aligned} \tilde{F}_{lin}(z_{0,0}^{(1)}, \dots, z_{K,L}^{(2)}, \zeta_{1,1}^{(1,1,1)}, \dots, \zeta_{K,L}^{(2,2,2)}, \eta_{0,0}, \dots, \eta_{K,L}, \sigma_{1,1}^{(x)}, \dots, \sigma_{K,L}^{(x)}, \sigma_{1,1}^{(y)}, \dots, \sigma_{K,L}^{(y)}) \\ = \frac{1}{2} \cdot \sum_{k=2}^{K-2} \sum_{l=2}^{L-2} \left[\varphi\left(\begin{pmatrix} z_{k-1,l-1}^{(1)} \\ z_{k-1,l-1}^{(2)} \end{pmatrix}, \begin{pmatrix} \zeta_{k,l}^{(1,1,1)} & \zeta_{k,l}^{(1,2,1)} \\ \zeta_{k,l}^{(2,1,1)} & \zeta_{k,l}^{(2,2,1)} \end{pmatrix}, \eta_{k-1,l-1}, \sigma_{k,l}^{(y)}, D\sigma_{k,l}^{(y)}, D^2\sigma_{k,l}^{(y)}, D\sigma_{k,l}^{(x)}\right) \right. \\ \left. + \varphi\left(\begin{pmatrix} z_{k,l}^{(1)} \\ z_{k,l}^{(2)} \end{pmatrix}, \begin{pmatrix} \zeta_{k,l}^{(1,1,2)} & \zeta_{k,l}^{(1,2,2)} \\ \zeta_{k,l}^{(2,1,2)} & \zeta_{k,l}^{(2,2,2)} \end{pmatrix}, \eta_{k,l}, \sigma_{k,l}^{(y)}, D\sigma_{k,l}^{(y)}, D^2\sigma_{k,l}^{(y)}, D\sigma_{k,l}^{(x)}\right) \right]. \end{aligned} \quad (4.24)$$

In complete analogy, $(R)_{joint,hyp}^N$ can be described. An appropriate ratio $\alpha : \beta$ for the global weights has been found by experiment. Note that, by the Weierstrass theorem, the discretized problems $(R)_{joint,lin}^N$ and $(R)_{joint,hyp}^N$ admit global minimizers.

5. Selected results.

a) Visualization and evaluation of the solutions.

After the determination of optimal solutions \hat{X}, \hat{Y} and (\hat{Z}, \hat{G}) of $(E)_1, (E)_2$ and $(R)_{lin} / (R)_{hyp}$ or an optimal solution $(\hat{X}, \hat{Y}, \hat{Z}, \hat{G})$ of $(R)_{joint,lin} / (R)_{joint,hyp}$, we calculate

$$J_{rek}(s) = J(s) - DJ(s)^T \hat{Z}(s) + \frac{1}{2} \hat{Z}(s)^T D^2 J(s) \hat{Z}(s); \quad (5.1)$$

$$S_{J,rek}(s) = S_{\hat{Y}}(s) - DS_{\hat{Y}}(s)^T \hat{Z}(s) + \frac{1}{2} \hat{Z}(s)^T D^2 S_{\hat{Y}}(s) \hat{Z}(s) + \frac{1}{6} \hat{G}(s) \cdot \|\hat{Z}(s)\|^3; \quad (5.2)$$

which will be considered as the corresponding reconstructions of the deformed template image $J(s - x(s))$ and the deformed template edge sketch $S_J(s - x(s))$. S_I will be represented by $S_{\hat{X}}$. Note that, within the following calculation of the indicators Q_0, \dots, Q_4 , a frame Ω_B dyed in black of 4 pixels width will be excluded.

The influence of the remainder $\frac{1}{6} \hat{G}(s) \cdot \|\hat{Z}(s)\|^3$ can be quantified by means of the indicator

$$Q_0(\hat{Z}, \hat{G}) = \max_{s \in \Omega \setminus \Omega_B} \left| \frac{1}{6} \hat{G}(s) \cdot \|\hat{Z}(s)\|^3 \right|. \quad (5.3)$$

In the experiments documented below, we get typically very small values of Q_0 .¹⁶⁾ Depending on the image data, experiments with values of $Q_0 \leq 0.02$ to $Q_0 \leq 0.08$ will be considered as reliable.

In the literature, there is no commonly accepted criterion for the evaluation of the results of multimodal registration. In most cases, the authors check the reliability of their calculations merely by a visual inspection of the results. In the present paper, in order to perform a quantitative evaluation of the results, we calculate three indicators. The first one is based on the correlation coefficient

$$CC(I, J) = \frac{\int_{\Omega \setminus \Omega_B} (I(s) - \tilde{I})(J(s) - \tilde{J}) ds}{\left(\int_{\Omega \setminus \Omega_B} (I(s) - \tilde{I})^2 ds \cdot \int_{\Omega \setminus \Omega_B} (J(s) - \tilde{J})^2 ds \right)^{1/2}} \quad (5.4)$$

with $\tilde{I} = \frac{1}{|\Omega \setminus \Omega_B|} \int_{\Omega \setminus \Omega_B} I(s) ds$ and $\tilde{J} = \frac{1}{|\Omega \setminus \Omega_B|} \int_{\Omega \setminus \Omega_B} J(s) ds$,

cf. [MODERSITZKI 04], p. 59 f., and [RICHTER 66], p. 263. Now the indicator

$$Q_1 = \left(CC(I, J_{rek}) - CC(I, J) \right) \cdot \frac{100\%}{CC(I, J)} \quad (5.5)$$

measures the improvement of the correlation between the images after applying the deformation \hat{Z} to J . In order to define the second indicator, we consider the definition (1.1) of the normalized gradient field of a given image. Then we may ask for the improvement of the average angular error

$$AAE(g_\sigma(I), g_\sigma(J)) = \frac{1}{|\Omega \setminus \Omega_B|} \int_{\Omega \setminus \Omega_B} \arccos \angle(g_\sigma(I(s)), g_\sigma(J(s))) ds \quad (5.6)$$

between the normalized gradient fields, which leads to the indicator

$$Q_2 = \left(AAE(g_\sigma(I), g_\sigma(J)) - AAE(g_\sigma(I), g_\sigma(J_{rek})) \right) \cdot \frac{100\%}{AAE(g_\sigma(I), g_\sigma(J))} \quad (5.7)$$

where $\sigma = 10^{-10}$ has been employed. The third indicator proposed here is the improvement of the relative reconstruction error of the edge sketches $S_{\hat{X}}, S_{\hat{Y}}$, which is expressed through their squared distance:

$$Q_3 = \left[\left(\int_{\Omega \setminus \Omega_B} (S_{\hat{X}}(s) - S_{\hat{Y}}(s))^2 ds \right)^{1/2} - \left(\int_{\Omega \setminus \Omega_B} (S_{\hat{X}}(s) - S_{J, rek}(s))^2 ds \right)^{1/2} \right] \cdot \frac{100\%}{\left(\int_{\Omega \setminus \Omega_B} (S_{\hat{X}}(s) - S_{\hat{Y}}(s))^2 ds \right)^{1/2}}. \quad (5.8)$$

¹⁶⁾ Note that a maximal grey value correction of a single step corresponds to $Q_0 \leq 1/255 \approx 0.0039$.

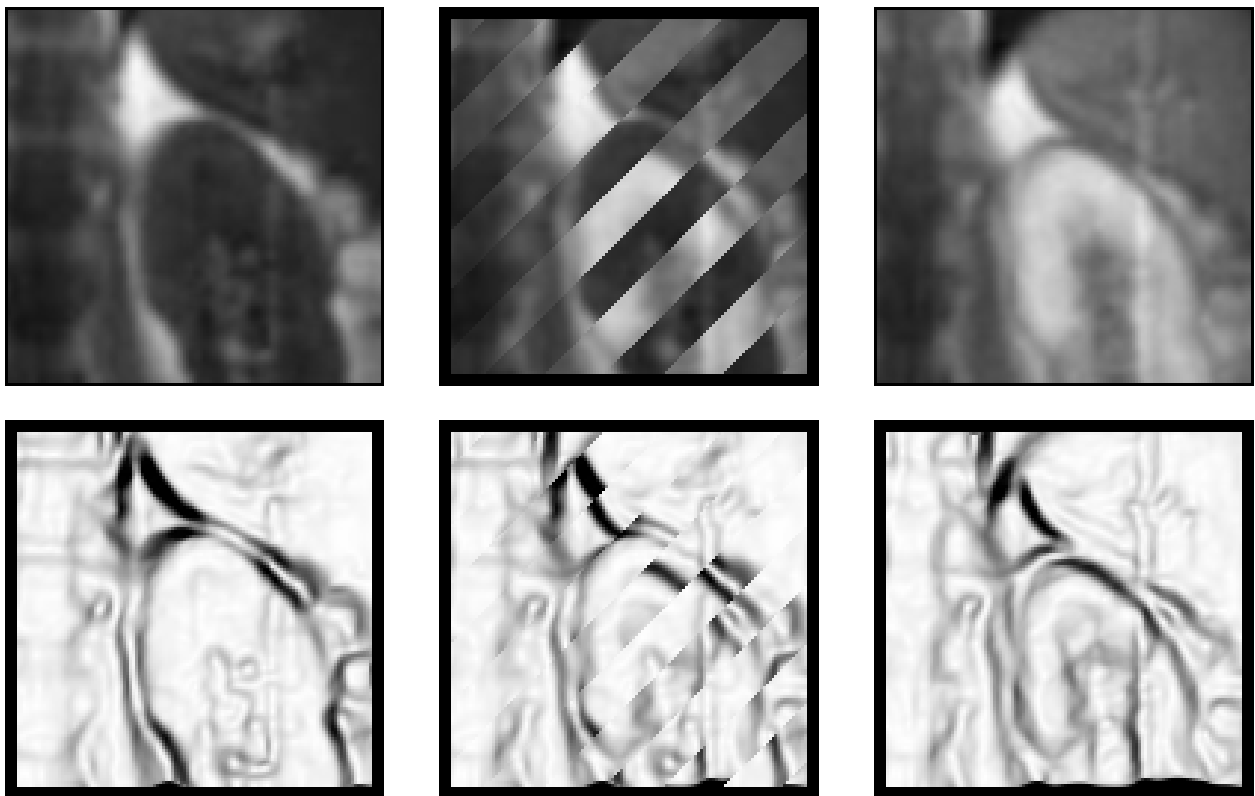
Note that all of the three indicators are allowed to take positive as well as negative values. As our experiments show, it is possible that the indicators will not move uniformly.

When visualizing the results of a particular experiment, we provide six images. First, we print the edge sketch $S_{\hat{\gamma}}$ of the template. Next, we produce an overlay of alternating stripes from the reconstructed template J_{rek} as calculated in (5.1) and the reference image I . We further visualize the deformation field \hat{Z} used for the generation of J_{rek} by a colorful orientation plot wherein the direction and the magnitude of the deformation vector is coded by the hue and intensity of a colored pixel. The correspondence between orientation and color can be read from the colored border (see e. g. Fig. 15).¹⁷⁾ In a second row, we will depict the edge sketches $S_{J,rek}$ and $S_{\hat{X}}$ of the reconstructed and the reference image left and right as well as their overlay with alternating stripes in the center.

b) Image data used in the experiments.

For the numerical experiments, we selected two image pairs from medical imaging, which represent both situations mentioned in the introduction.

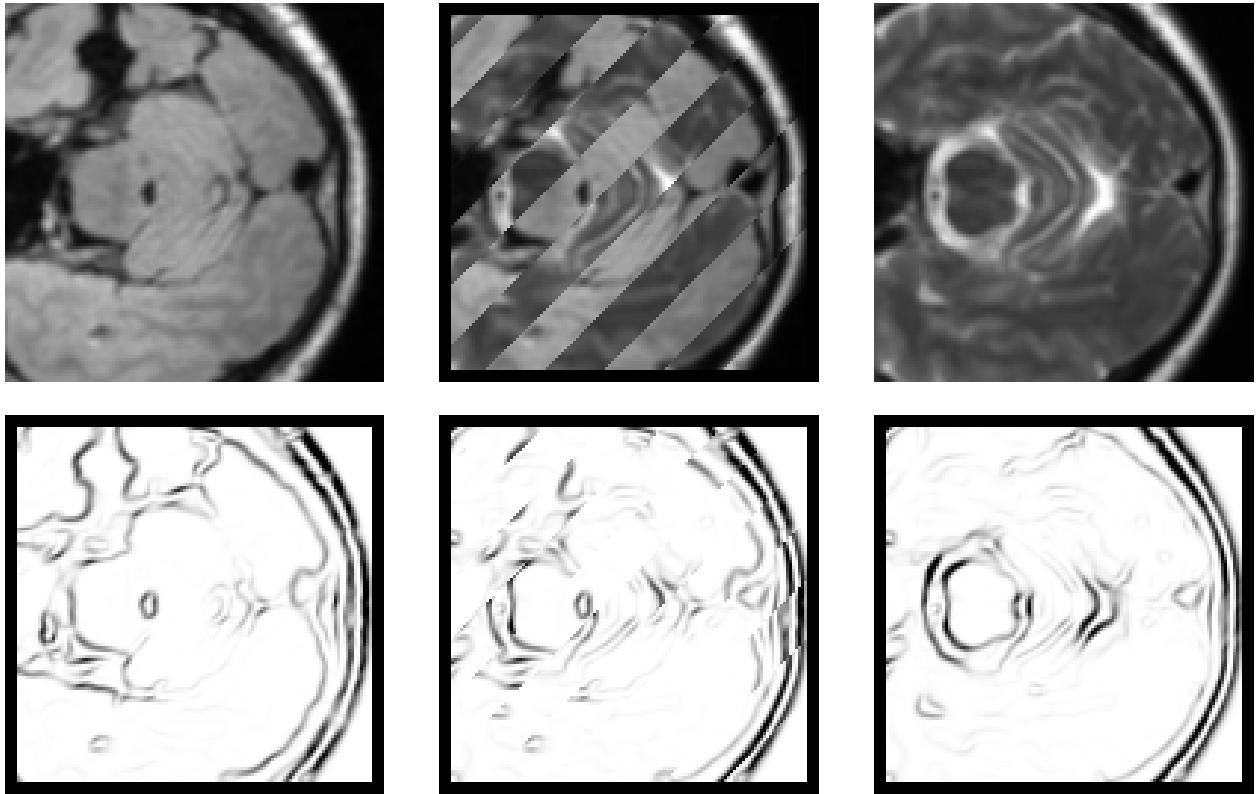
Image pair 1: MR tomography of the kidney region, cut-out.



Figs. 1 – 6. Top left: template J . Top center: overlay of I and J in alternating stripes. Top right: reference image I . Bottom left: edge sketch S_J . Bottom center: overlay of S_I and S_J in alternating stripes. Bottom right: edge sketch S_I .

¹⁷⁾ The visualization has been realized using a HSI color model where every color is represented by the three coordinates hue, saturation and intensity, cf. [BRUNE/MAURER/WAGNER 09], p. 1197, and [PLATANIOTIS/VENETSANOPOULOS 00], pp. 25 ff. Since we need only two coordinates for the visualization of the deformation field \hat{Z} , the saturation has been left constant.

Image pair 2: MR tomography of the human brain, cut-out.



Figs. 7 – 12. Top left: template J . Top center: overlay of I and J in alternating stripes. Top right: reference image I . Bottom left: edge sketch S_J . Bottom center: overlay of S_I and S_J in alternating stripes. Bottom right: edge sketch S_I .

The first pair (Figs. 1 and 3), generated as subsequent frames by MR tomography with a single device and the same protocol, shows a coronal section through the left kidney and, in the left half of the images, a part of the spine. The difference in the modality is caused by application of a contrast agent in the meantime.¹⁸⁾ The second pair (Figs. 7 and 9) is generated by MR tomography with different imaging protocols (Flair, T_2) and shows an axial section through the human brain.¹⁹⁾ In both pairs, the original data have been presmoothed by (3×3) -averaging. The edge sketches (Figs. 4, 6, 10 and 12) have been generated by (2.5) and (2.6) from solutions of $(E)_1$ and $(E)_2$ with $\lambda = 0.05$, $\delta = 0.01$, $R = 0.2$ and $n = 4$. The sizes of the pairs amount to 128×128 pixels with a frame of 4 pixels width dyed in black.

c) Results of the separated access.

We document first a selection of results of the separated strategy. In the tables, the experiments have been sorted by decreasing regularization parameter μ . The star (*) indicates that the results are imaged in Subsection 5.e) below.

¹⁸⁾ Images courtesy of Prof. R. STOLLBERGER (TU Graz, Institute of Medical Engineering) and Dr. M. ASCHAUER (Medical University of Graz, Division of Vascular and Interventional Radiology). From a contrast-modulated sequence comprising 135 frames in total, cutouts of the frames #03 and #54 have been selected.

¹⁹⁾ Images courtesy of Dr. B. H. MENZE (ETH Zürich, Computer Vision Laboratory), frames #flair_2008_07_18_138 and #t2_2008_07_18_144, cutouts.

Table 1. Linear-elastic registration of image pair 1 by subsequent solution of $(E)_1$, $(E)_2$ and $(R)_{lin}$. The parameters $\lambda = 0.05$, $\delta = 0.01$, $R = 0.1$, $\varepsilon = 10^{-6}$ and $\eta_{max} = 0.001$ have been used.

Exper. No.	μ	T	Q_0	Q_1	Q_2	Q_3
01	0.060	8.0	0.0070	17.10	0.47	10.91
02	0.060	0.8	0.0069	14.19	0.28	10.64
03	0.060	0.2	0.0039	11.07	-0.04	7.81
04 (*)	0.020	8.0	0.0585	18.85	0.73	20.78

Table 2. Linear-elastic registration of image pair 2 by subsequent solution of $(E)_1$, $(E)_2$ and $(R)_{lin}$. The parameters $\lambda = 0.05$, $\delta = 0.01$, $R = 0.1$, $\varepsilon = 10^{-6}$ and $\eta_{max} = 0.001$ have been used.

Exper. No.	μ	T	Q_0	Q_1	Q_2	Q_3
05	0.060	8.0	0.0029	4.41	6.38	14.21
06	0.060	0.8	0.0034	3.31	5.46	12.52
07	0.060	0.2	0.0025	3.69	5.31	10.03
08	0.020	8.0	0.0086	2.68	6.68	20.49
09 (*)	0.008	8.0	0.0161	1.38	6.61	28.51
10	0.002	8.0	0.1606	0.19	7.13	43.90

Table 3. Hyperelastic registration of image pair 1 by subsequent solution of $(E)_1$, $(E)_2$ and $(R)_{hyp}$. The parameters $\lambda = 0.05$, $\delta = 0.01$, $R = 0.2$, $\gamma_1 = 0.05$, $\gamma_2 = 0.25$, $p = 2$ and $\eta_{max} = 0.001$ have been used.

Exper. No.	μ	T	Q_0	Q_1	Q_2	Q_3
11	0.800	8.0	0.0021	7.42	0.07	4.62
12	0.500	8.0	0.0036	9.56	0.24	6.26
13 (*)	0.200	8.0	0.0081	13.48	0.55	10.82
14	0.020	8.0	0.2732	15.15	1.51	32.62

Table 4. Hyperelastic registration of image pair 2 by subsequent solution of $(E)_1$, $(E)_2$ and $(R)_{hyp}$. The parameters $\lambda = 0.05$, $\delta = 0.01$, $R = 0.2$, $\gamma_1 = 0.05$, $\gamma_2 = 0.25$, $p = 2$ and $\eta_{max} = 0.001$ have been used.

Exper. No.	μ	T	Q_0	Q_1	Q_2	Q_3
15	0.800	8.0	0.0022	4.59	5.81	11.61
16	0.200	8.0	0.0074	3.25	6.79	17.91
17	0.070	8.0	0.0183	1.96	6.53	24.98
18 (*)	0.020	8.0	0.0664	1.47	7.37	34.55

d) Results of the joint access.

Here we document numerical solutions of the joint problems $(R)_{joint,lin}$ and $(R)_{joint,hyp}$. The experiments have been sorted by decreasing regularization parameter μ again.

Table 5. Linear-elastic registration of image pair 1 by solution of $(R)_{joint,lin}$. The parameters $\alpha = 6000$, $\beta = 1$, $\delta = 0.01$, $\varepsilon = 10^{-6}$ and $\eta_{max} = 0.001$ have been used. In Experiments 20 – 22, the edge sketches have been generated with $n = 2$ instead of $n = 4$.

Exp. No.	λ	R	μ	T	Q_0	Q_1	Q_2	Q_3
19 (*)	0.05	0.10	0.06	8.0	0.0125	10.90	0.07	9.13
20	0.05	0.30	0.04	8.0	0.0091	9.73	-0.44	6.36
21	0.05	0.20	0.04	8.0	0.0096	10.30	-0.26	9.00
22 (*)	0.05	0.10	0.04	8.0	0.0303	12.57	-0.25	13.81

Table 6. Linear-elastic registration of image pair 2 by solution of $(R)_{joint,lin}$. The parameters $\alpha = 6000$, $\beta = 1$, $\delta = 0.01$, $\varepsilon = 10^{-6}$ and $\eta_{max} = 0.001$ have been used. In Experiment 25, the edge sketches have been generated with $n = 2$ instead of $n = 4$.

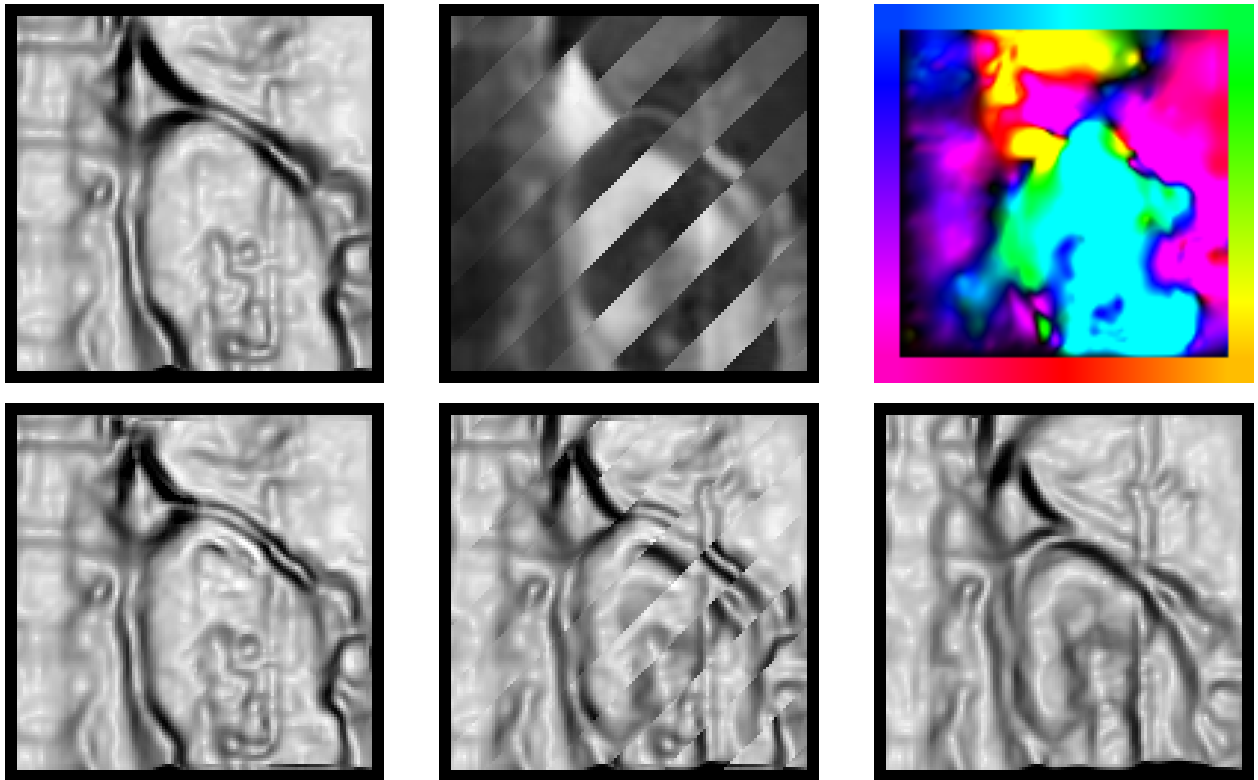
Exp. No.	λ	R	μ	T	Q_0	Q_1	Q_2	Q_3
23	0.05	0.20	0.060	8.0	0.0001	4.97	3.70	14.97
24	0.05	0.20	0.040	8.0	0.0078	4.46	4.33	17.51
25 (*)	0.05	0.20	0.040	8.0	0.0115	4.20	4.06	20.93
26	0.05	0.20	0.020	8.0	0.0123	4.03	4.47	22.17
27	0.05	0.20	0.008	8.0	0.0308	3.78	4.98	30.10

Table 7. Hyperelastic registration of image pair 2 by solution of $(R)_{joint,hyp}$. The parameters $\alpha = 6000$, $\beta = 1$, $\delta = 0.01$, $\varepsilon = 10^{-6}$, $\gamma_1 = 0.05$, $\gamma_2 = 0.25$, $p = 2$ and $\eta_{max} = 0.001$ have been used.

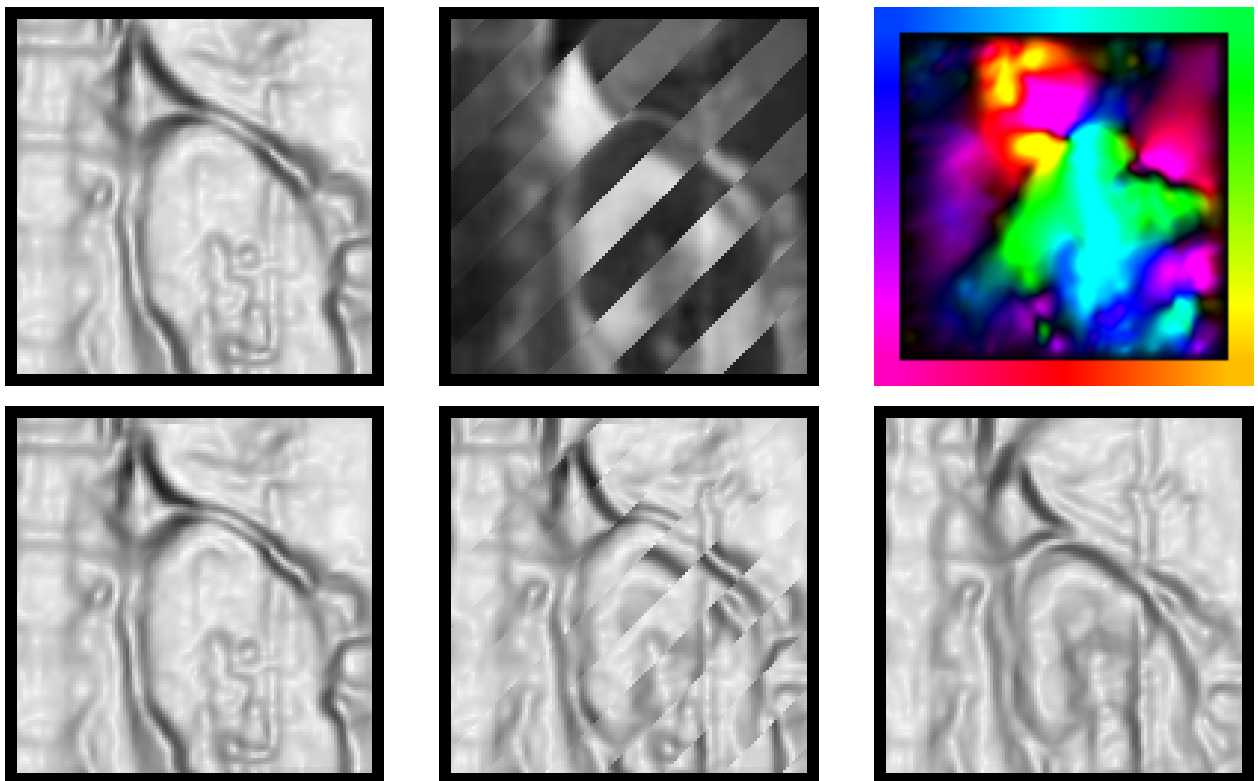
Exp. No.	λ	R	μ	T	Q_0	Q_1	Q_2	Q_3
28	0.05	0.20	0.800	8.0	0.0000	6.24	3.05	7.94
29	0.05	0.20	0.500	8.0	0.0017	5.77	3.47	8.95
30	0.05	0.20	0.200	8.0	0.0008	5.80	3.05	10.15
31 (*)	0.05	0.20	0.002	8.0	0.0635	3.57	5.23	39.18

e) Visualization of selected results.

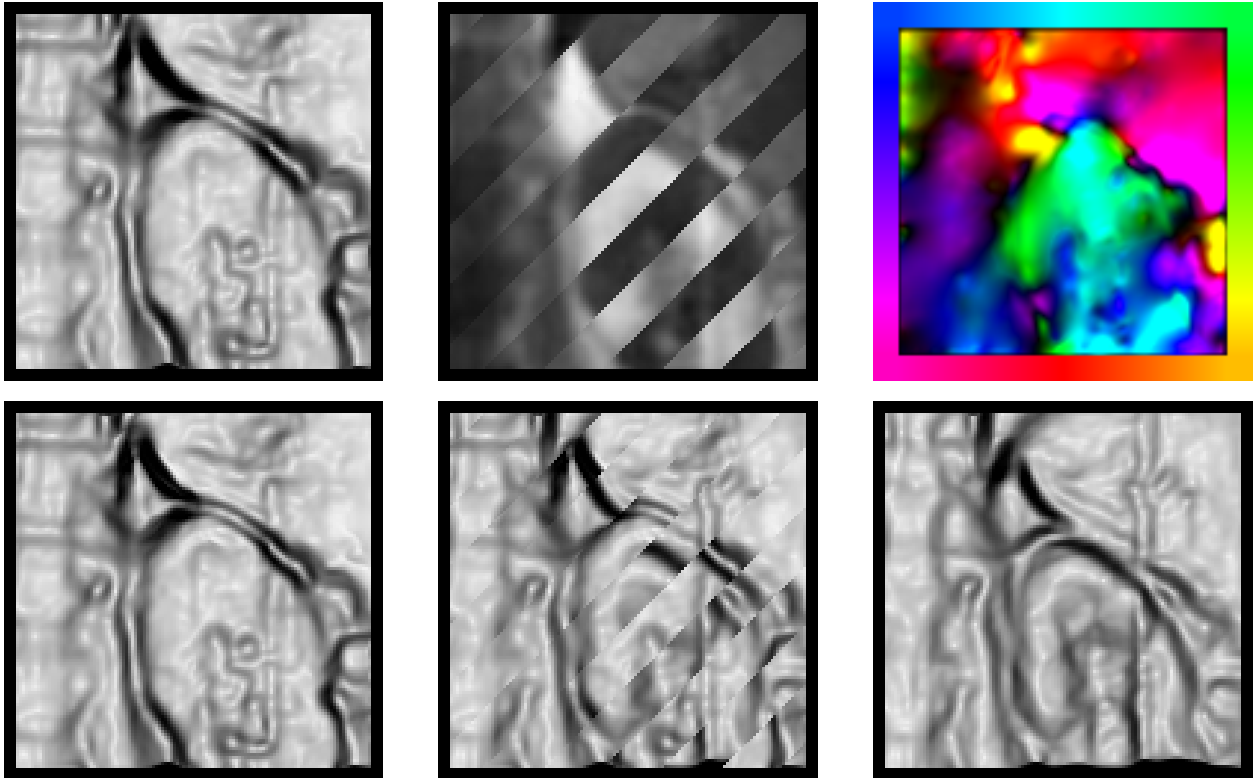
In Figs. 13 – 36, we show the results of Experiments 04, 13, 19 and 22 with image pair 1. In Figs. 37 – 60, the results of Experiments 09, 18, 25 and 31 with image pair 2 are documented.



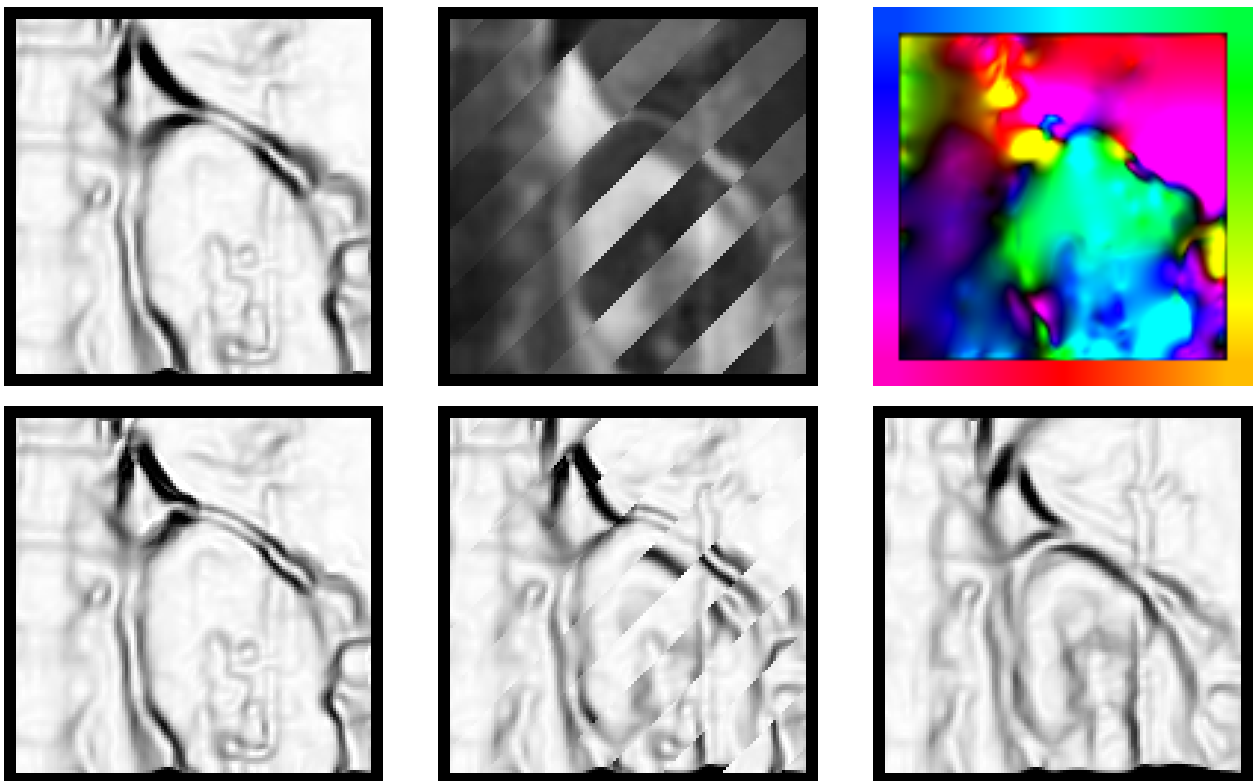
Figs. 13 – 18. Results of Experiment No. 04 (image pair 1, linear-elastic registration, separated access). Top left: edge sketch S_Y . Top center: overlay of J_{rek} and I . Top right: color plot of \hat{Z} . Bottom left: edge sketch $S_{J,rek}$. Bottom center: overlay of $S_{J,rek}$ and $S_{\hat{X}}$. Bottom right: edge sketch $S_{\hat{X}}$.



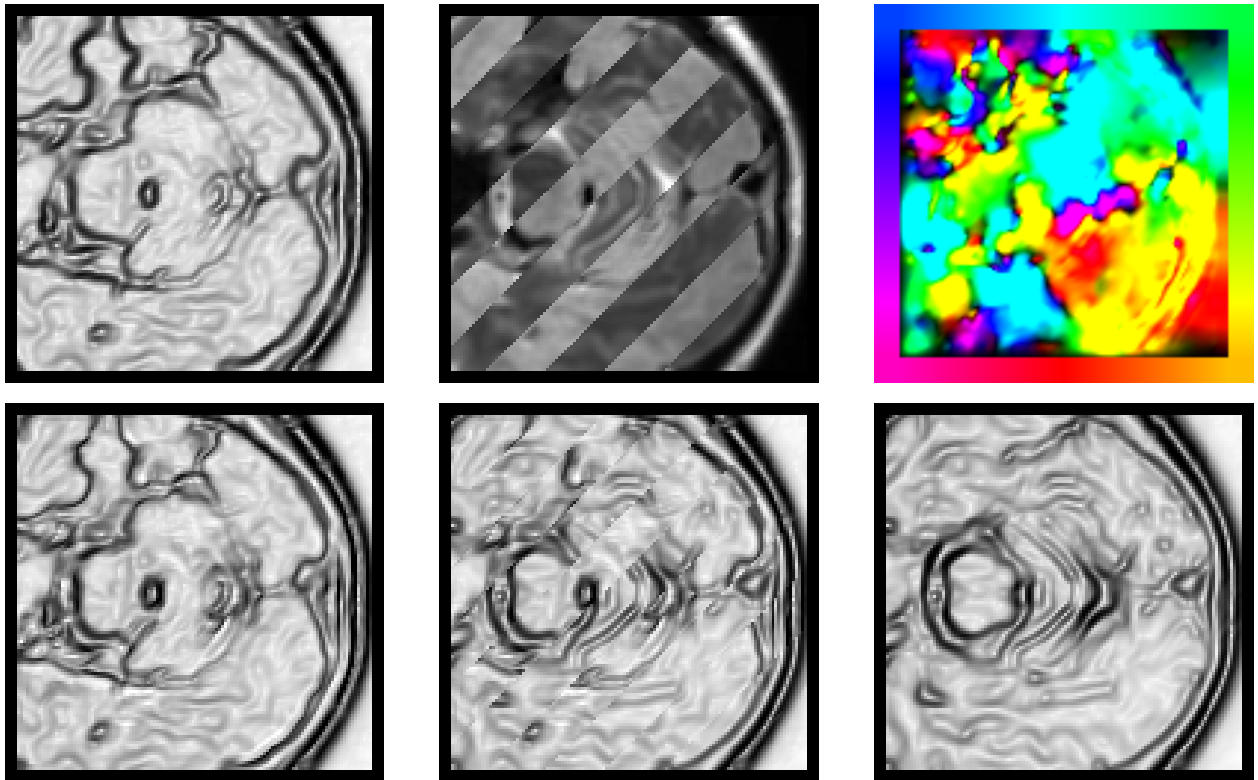
Figs. 19 – 24. Results of Experiment No. 13 (image pair 1, hyperelastic registration, separated access). Top left: edge sketch S_Y . Top center: overlay of J_{rek} and I . Top right: color plot of \hat{Z} . Bottom left: edge sketch $S_{J,rek}$. Bottom center: overlay of $S_{J,rek}$ and $S_{\hat{X}}$. Bottom right: edge sketch $S_{\hat{X}}$.



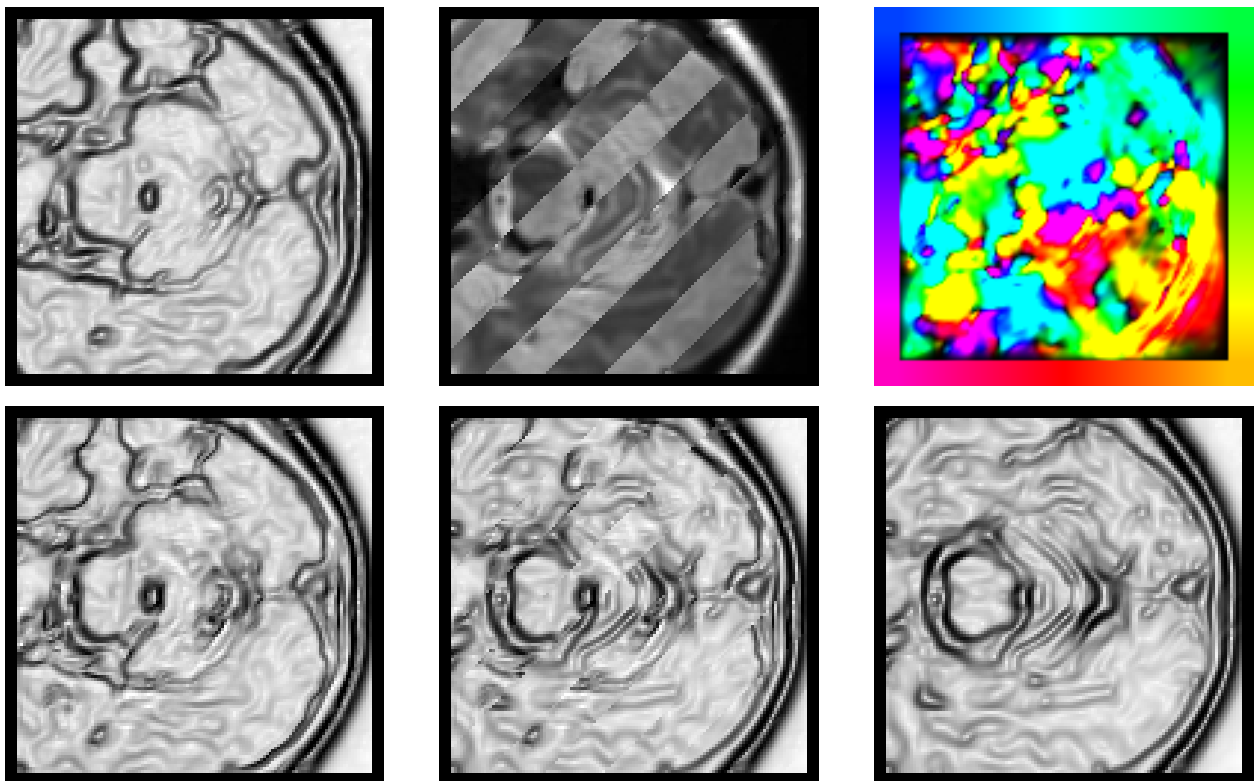
Figs. 25 – 30. Results of Experiment No. 19 (image pair 1, linear-elastic registration, joint access). Top left: edge sketch $S_{\hat{Y}}$. Top center: overlay of J_{rek} and I . Top right: color plot of \hat{Z} . Bottom left: edge sketch $S_{J,rek}$. Bottom center: overlay of $S_{J,rek}$ and $S_{\hat{X}}$. Bottom right: edge sketch $S_{\hat{X}}$.



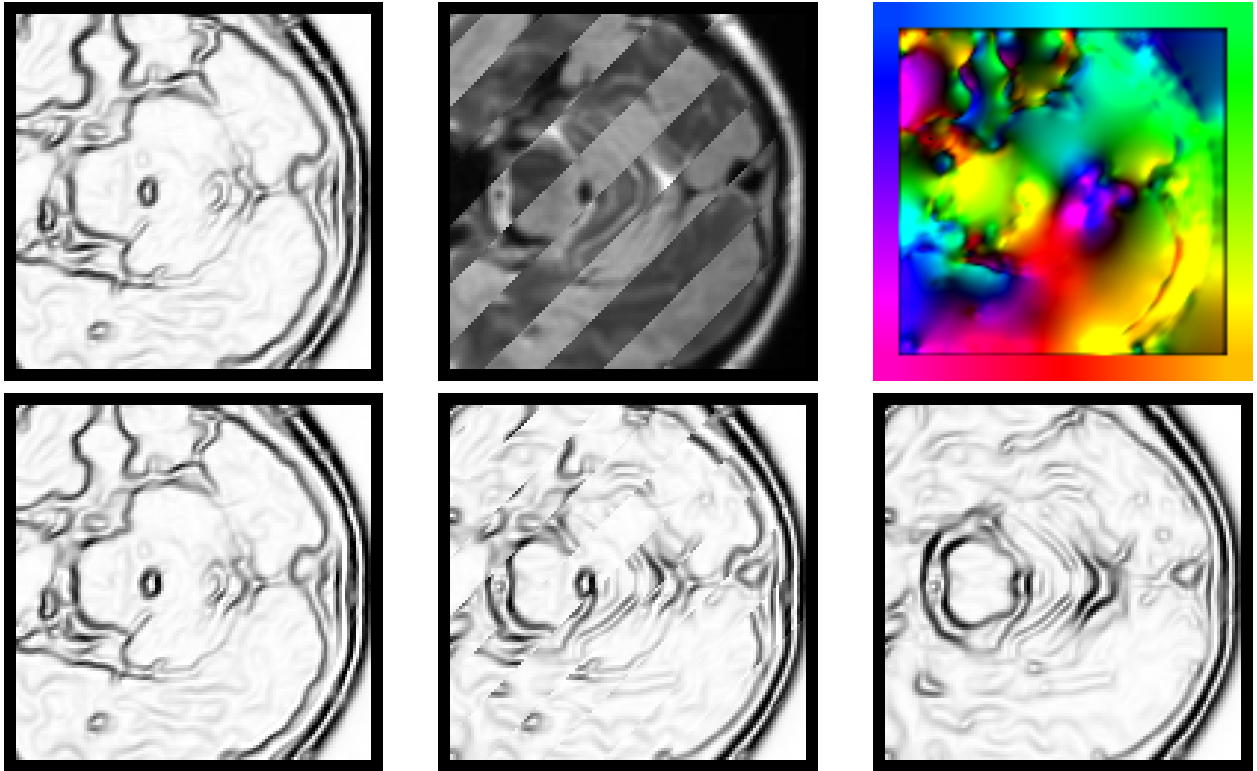
Figs. 31 – 36. Results of Experiment No. 22 (image pair 1, linear-elastic registration, joint access). Top left: edge sketch $S_{\hat{Y}}$. Top center: overlay of J_{rek} and I . Top right: color plot of \hat{Z} . Bottom left: edge sketch $S_{J,rek}$. Bottom center: overlay of $S_{J,rek}$ and $S_{\hat{X}}$. Bottom right: edge sketch $S_{\hat{X}}$.



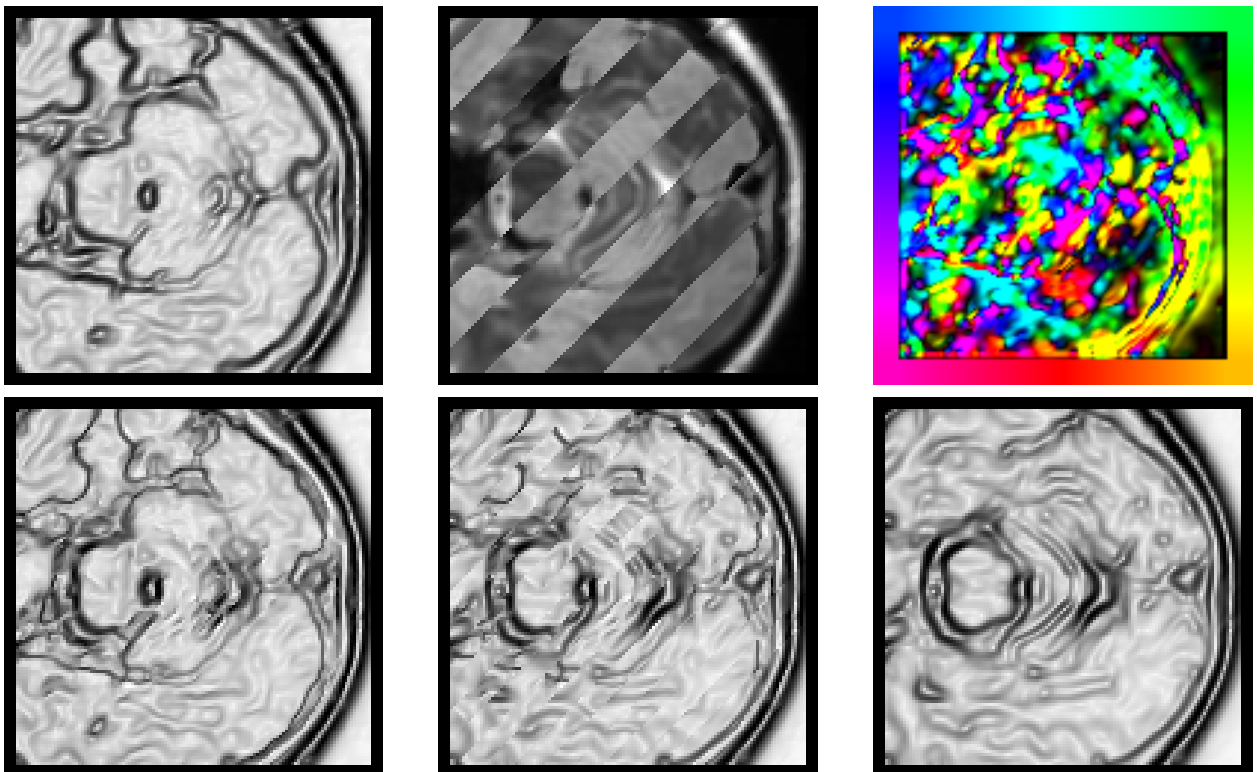
Figs. 37 – 42. Results of Experiment No. 09 (image pair 2, linear-elastic registration, separated access). Top left: edge sketch S_Y . Top center: overlay of J_{rek} and I . Top right: color plot of \hat{Z} . Bottom left: edge sketch $S_{J,rek}$. Bottom center: overlay of $S_{J,rek}$ and $S_{\hat{X}}$. Bottom right: edge sketch $S_{\hat{X}}$.



Figs. 43 – 48. Results of Experiment 18 (image pair 2, hyperelastic registration, separated access). Top left: edge sketch S_Y . Top center: overlay of J_{rek} and I . Top right: color plot of \hat{Z} . Bottom left: edge sketch $S_{J,rek}$. Bottom center: overlay of $S_{J,rek}$ and $S_{\hat{X}}$. Bottom right: edge sketch $S_{\hat{X}}$.



Figs. 49 – 54. Results of Experiment No. 25 (image pair 2, linear-elastic registration, joint access). Top left: edge sketch $S_{\hat{Y}}$. Top center: overlay of J_{rek} and I . Top right: color plot of \hat{Z} . Bottom left: edge sketch $S_{J,rek}$. Bottom center: overlay of $S_{J,rek}$ and $S_{\hat{X}}$. Bottom right: edge sketch $S_{\hat{X}}$.



Figs. 55 – 60. Results of Experiment No. 31 (image pair 2, hyperelastic registration, joint access). Top left: edge sketch $S_{\hat{Y}}$. Top center: overlay of J_{rek} and I . Top right: color plot of \hat{Z} . Bottom left: edge sketch $S_{J,rek}$. Bottom center: overlay of $S_{J,rek}$ and $S_{\hat{X}}$. Bottom right: edge sketch $S_{\hat{X}}$.

f) Reference solutions from the variational method FAIR.

For purpose of comparison, the pairs have been fed into the toolbox FAIR distributed with [MODERSITZKI 09], which accounts for a variational access to image registration and its numerical solution. The variational problem solved there reads as follows:

$$(V) \quad F_{var}(Z) = \int_{\Omega} \left(1 - (g_{\sigma}(I(s))^T g_{\sigma}(J(Z(s)))) \right)^2 ds \quad (5.9)$$

$$+ \frac{\nu_1}{2} \int_{\Omega} \left(\nu_2 (\nabla Z_1(s))^2 + \nabla Z_2(s)^2 \right) + (\nu_2 + \nu_3) (\operatorname{div} Z(s))^2 ds \longrightarrow \inf!;$$

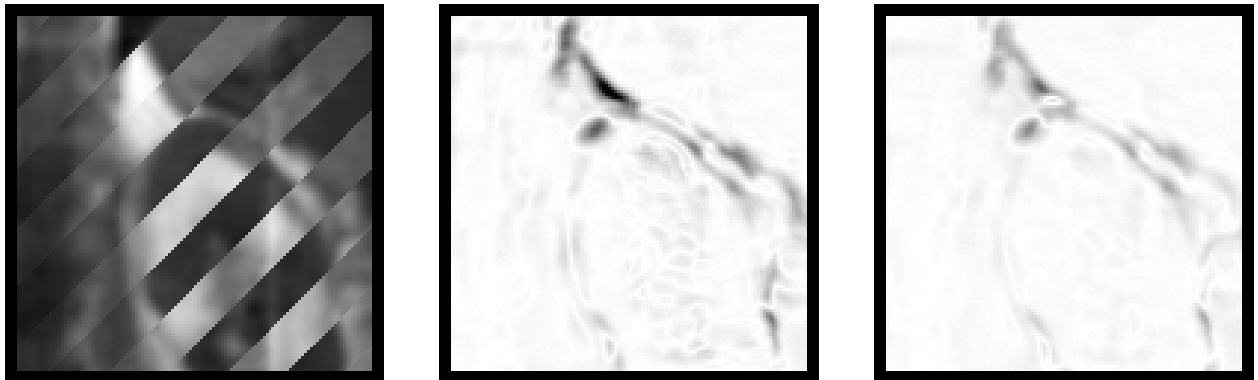
$$Z \in W_0^{1,p}(\Omega, \mathbb{R}^2) \quad (5.10)$$

with a regularization parameter $\nu_1 > 0$ and weights $\nu_2, \nu_3 > 0$.²⁰⁾ The best results obtained this way will be documented in the following table.

Table 8. Linear-elastic registration of image pairs 1 and 2 by solving (V) with FAIR. The parameters $\nu_2 = 1$ and $\nu_3 = 0$ have been used.

Exp. No.	Image pair	Preregistration	ν_1	Q_1	Q_2	Q_3
32 (*)	1	no	0.005	4.68	-0.00	n/a
33	1	yes	0.010	3.43	0.12	n/a
34	2	no	0.005	7.28	4.83	n/a
35 (*)	2	no	0.010	6.52	5.02	n/a

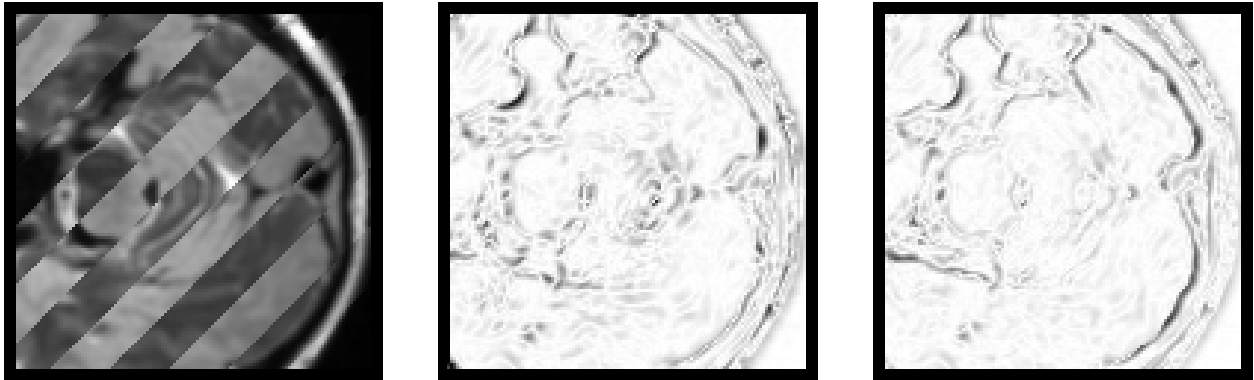
On the level of the visual comparison of the reconstructed images, the differences between the results of the optimal control access and the variational method FAIR as reference method are subtle. In order to make them visible, we document the results of Experiments 32 and 35 by overlay of alternating diagonal stripes (Figs. 61 and 64, which may be compared e. g. with Figs. 14 and 44). In Figs. 62 – 63 and 65 – 66, we depict the grey value difference²¹⁾ between the reconstructed templates $J(Z(s))$ generated by FAIR and J_{rek} generated in Experiments 04, 22, 18 and 31 with the optimal control problems, respectively.



Figs. 61 – 63. Left: result of Experiment No. 32 (image pair 1, linear-elastic registration with FAIR). Center: comparison of the results of Experiments Nos. 32 and 04 (image pair 1, linear-elastic registration with FAIR / linear-elastic registration, separated control access). Right: comparison of the results of Experiments Nos. 32 and 22 (image pair 1, linear-elastic registration with FAIR / linear-elastic registration, joint control access).

²⁰⁾ Unfortunately, FAIR does not contain an implementation of a hyperelastic regularizer. The paper [BURGER/MODERSITZKI/RUTHOTTO 13], which is concerned with a related hyperelastic method, came not to the attention of the authors until the present investigation has been finished.

²¹⁾ The differences have been magnified by factor 2.



Figs. 64 – 66. Left: result of Experiment No. 35 (image pair 2, linear-elastic registration with FAIR). Center: comparison of the results of Experiments Nos. 35 and 18 (image pair 2, linear-elastic registration with FAIR / hyperelastic registration, separated control access). Right: comparison of the results of Experiments Nos. 35 and 31 (image pair 2, linear-elastic registration with FAIR / hyperelastic registration, joint control access).

g) Discussion of the results.

In general, a visual inspection of the results shows a quite satisfactory alignment of features in the separated as well as in the joint access for both image pairs (Figs. 14, 20, 26, 32, 38, 44, 50 and 56). In comparison with the output of FAIR, subtle differences are present but hardly visible at the first glance.

The behaviour of the indicators reflects the principal difficulty of adequate quantitative evaluation of the results of multimodal matching. For image pair 1, we get $Q_1 \in [11.07, 18.85]$, $Q_1 \in [7.42, 15.15]$ and $Q_1 \in [9.73, 12.57]$ for the optimal control approach with $(R)_{lin}$, $(R)_{hyp}$ and $(R)_{joint,lin}$, respectively. For image pair 2, within the problems $(R)_{lin}$, $(R)_{hyp}$, $(R)_{joint,lin}$ and $(R)_{joint,hyp}$, we obtain $Q_1 \in [0.19, 4.41]$, $Q_1 \in [1.47, 4.59]$, $Q_1 \in [4.03, 4.97]$, and $Q_1 \in [3.57, 6.24]$. On the other hand, the improvement of the AAE between the normalized gradient fields for image pair 1 is quite small (if any), as documented by $Q_2 \in [-0.04, 0.73]$, $Q_2 \in [0.07, 1.51]$ and $Q_2 \in [-0.44, 0.07]$ while the experiments for image pair 2 give moderate improvements of $Q_2 \in [5.31, 7.13]$, $Q_2 \in [5.81, 7.37]$, $Q_2 \in [3.70, 4.98]$ and $Q_2 \in [3.05, 5.23]$. A comparison with the output of the variational method FAIR shows that these values compete well, given $Q_1 \in [3.43, 4.68]$, $Q_2 \in [-0.00, 0.12]$ for image pair 1 and $Q_1 \in [6.52, 7.28]$, $Q_2 \in [4.83, 5.02]$ for image pair 2 produced by this method. The fact that the control access gives in many cases slightly better indicator values than FAIR may be attributed to the fact that the use of weighted edge sketches instead of normalized gradient fields leads to a potential suppression of “unnecessary” details, thus granting more freedom in the search of a matching deformation. On the other hand, in some cases the deformation fields obtained are quite fragmented (compare e. g. Fig. 57 with Fig. 39). The alignment of the edge sketches, as to be expected, is not as precise as in comparable experiments of unimodal matching but reaches in the best cases about 40% (Experiments 10 and 31). Typical values of Q_3 lie around 15 – 20%.

The expectation that the joint access leads to a refinement of the results of the separated access is only partly confirmed. For image pair 1, the joint access gives inferior results with respect to Q_1 and Q_2 and roughly the same values of Q_3 ; for image pair 2, the joint access ameliorates Q_1 but loses quality in Q_2 . Concerning Q_3 , the better values will be produced in the linear-elastic case by the separated access and in the hyperelastic case by the joint access. It seems that the advantage of the joint access is often counterweighted by a loss of numerical stability.

Concerning the runtime behaviour, the AMPL/IPOPT configuration is surely not an optimal one. A considerable speedup may be expected if the problems will be treated with e.g. semismooth Newton methods,

cf. e. g. [CLASON/JIN/KUNISCH 10] (this will be done in the future). As to be expected, the separated access runs remarkably faster than the joint access due to the very fast convergence of approximate solutions to the optimal edge sketch in $(E)_1^N$ and $(E)_2^N$, which allows for stopping after 5 – 10 iteration steps of IPOPT. The selection of the regularization parameters λ , μ and the control parameters R , T (which, in fact, act as additional regularization parameters) has been made by experiment but could be done automatically as well.²²⁾

h) Conclusion and outlook.

We may summarize that the presented optimal control approach, exploiting the image geometry by use of weighted edge sketches instead of normalized gradient fields, provides a reliable method of multimodal image registration. The results compete well with output of existing variational methods like FAIR, leading in some cases even to slight improvements. In the best cases, the correlation between the images and the average angular error have been improved by about 19% and 7%, respectively, while the alignment of the edge sketches may be improved by up to 40%. A joint access to edge detection and elastic matching was expected to produce finer results but experiments confirmed this only partly.

The presented approach may surely be improved under different viewpoints. This concerns the specification of the underlying elasticity models as well as the choice of the fidelity term, the discretization strategy and the implementation of the solver for the system of the first-order conditions. In particular, a replacement of the interior-point solver by a semismooth Newton solver seems to be advisable in the future.

Acknowledgment.

We wish to thank Prof. H. Maurer (Münster), who suggested to approach multidimensional control problems by direct methods and strongly encouraged the present investigation. Further, we would like to thank Prof. R. Stollberger (Graz) and M. Aschauer (Graz) as well as B. Menze (Zürich) who kindly provided us with tomographic image data. The present work has been supported within the project “Relaxation theorems and necessary optimality conditions for semiconvex multidimensional control problems” by the German Research Council.

References.

1. [ANGELOV 11] Angelov, A.: *Multimodale Bildregistrierung durch elastisches Matching von Kantenskizzen*. Diploma thesis; University of Münster 2011
2. [BOURDIN 99] Bourdin, B.: *Image segmentation with a finite element method*. M2AN Mathematical Modelling and Numerical Analysis **33** (1999), 229 – 244
3. [BRUNE/MAURER/WAGNER 09] Brune, C.; Maurer, H.; Wagner, M.: *Detection of intensity and motion edges within optical flow via multidimensional control*. SIAM J. Imaging Sci. **2** (2009), 1190 – 1210
4. [BURGER/MODERSITZKI/RUTHOTTO 13] Burger, M.; Modersitzki, J.; Ruthotto, L.: *A hyperelastic regularization energy for image registration*. SIAM J. Sci. Comput. **35** (2013), B132 – B148
5. [CLASON/JIN/KUNISCH 10] Clason, C.; Jin, B.; Kunisch, K.: *A semismooth Newton method for L^1 data fitting with automatic choice of regularization parameters and noise calibration*. SIAM J. Imaging Sci. **3** (2010), 199 – 231

²²⁾ E. g. by a training method along the lines of [MIN/POWELL/BOWYER 04] or using an adaptive strategy as described in [CLASON/JIN/KUNISCH 10], pp. 1492 ff.

-
6. [DACOROGNA 08] Dacorogna, B.: *Direct Methods in the Calculus of Variations*. Springer; New York etc. 2008, 2nd ed.
 7. [DROSKE/RUMPF 04] Droske, M.; Rumpf, M.: *A variational approach to nonrigid morphological image registration*. SIAM J. Appl. Math. **64** (2004), 668 – 687
 8. [DROSKE/RUMPF 07] Droske, M.; Rumpf, M.: *Multiscale joint segmentation and registration of image morphology*. IEEE Trans. Pattern Recognition Machine Intelligence **29** (2007), 2181 – 2194
 9. [EVANS/GARIEPY 92] Evans, L. C.; Gariepy, R. F.: *Measure Theory and Fine Properties of Functions*. CRC Press; Boca Raton etc. 1992
 10. [FISCHER/MODERSITZKI 03] Fischer, B.; Modersitzki, J.: *Curvature based image registration*. J. Math. Imaging Vision **18** (2003), 81 – 85
 11. [FOURER/GAY/KERNIGHAN 03] Fourer, R.; Gay, D. M.; Kernighan, B. W.: *AMPL. A Modeling Language for Mathematical Programming*. Brooks/Cole — Thomson Learning; Pacific Grove 2003, 2nd ed.
 12. [FRANEK/FRANEK/MAURER/WAGNER 12] Franek, L.; Franek, M.; Maurer, H.; Wagner, M.: *A discretization method for the numerical solution of Dieudonné-Rashevsky type problems with application to edge detection within noisy image data*. Opt. Control Appl. Meth. **33** (2012), 276 – 301
 13. [GALLARDO/MEJU 05] Gallardo, L. A.; Meju, M. A.; Pérez-Flores, M. A.: *A quadratic programming approach for joint image reconstruction: mathematical and geophysical examples*. Inverse Problems **21** (2005), 435 – 452
 14. [GOERING/ROOS/TOBISKA 93] Goering, H.; Roos, H.-G.; Tobiska, L.: *Finite-Element-Method*. Akademie-Verlag; Berlin 1993, 3rd ed.
 15. [HABER/MODERSITZKI 07] Haber, E.; Modersitzki, J.: *Intensity gradient based registration and fusion of multimodal images*. Methods of Information in Medicine **46** (2007), 292 – 299
 16. [HAN ET AL. 06] Han, J.; Berkels, B.; Rumpf, M.; Hornegger, J.; Droske, M.; Fried, M.; Scorzin, J.; Schaller, C.: *A variational framework for joint image registration, denoising and edge detection*. In: Handels, H.; Ehrhardt, J.; Horsch, A.; Meinzer, H.-P.; Tolxdorff, T.: *Bildverarbeitung für die Medizin 2006*. Springer; Berlin etc. 2006, 246 – 250
 17. [HENN/WITSCH 01] Henn, S.; Witsch, K.: *Iterative multigrid regularization techniques for image matching*. SIAM J. Sci. Comput. **23** (2001), 1077 – 1093
 18. [HERMOSILLO/CHEFD'HOTEL/FAUGERAS 02] Hermosillo, G.; Chefd'hotel, C.; Faugeras, O.: *Variational methods for multimodal image matching*. Int. J. Computer Vision **50** (2002), 329 – 343
 19. [HINTERMÜLLER/KEELING 09] Hintermüller, M.; Keeling, S. L.: *Image registration and segmentation based on energy minimization*. In: Pardalos, P. M.; Romeijn, H. E. (Eds.): *Handbook of Optimization in Medicine*. Springer; New York 2009, 213 – 252
 20. [JANSEN 97] Jansen, B.: *Interior Point Techniques in Optimization*. Kluwer; Dordrecht 1997
 21. [LAIRD/WÄCHTER 09] Laird, C.; Wächter, A.: *Introduction to IPOPT: A tutorial for downloading, installing, and using IPOPT. Revision No. 1830*. Electronically published: <https://www.coin-or.org/Ipopt/export/2158/stable/3.9/Ipopt/doc/documentation.pdf> (accessed at 15.12.2012)
 22. [MIN/POWELL/BOWYER 04] Min, J.; Powell, M.; Bowyer, K. W.: *Automated performance evaluation of range image segmentation algorithms*. IEEE Trans. Systems, Man, and Cybernetics, Part B **34** (2004), 263 – 271
 23. [MODERSITZKI 04] Modersitzki, J.: *Numerical Methods for Image Registration*. Oxford University Press; Oxford 2004
 24. [MODERSITZKI 09] Modersitzki, J.: *FAIR. Flexible Algorithms for Image Registration*. SIAM; Philadelphia 2009
 25. [OGDEN 03] Ogden, R. W.: *Nonlinear elasticity, anisotropy, material stability and residual stresses in soft tissue*. In: Holzapfel, G. A.; Ogden, R. W. (Eds.): *Biomechanics of Soft Tissue in Cardiovascular Systems*. Springer; Wien etc. 2003, 65 – 108
 26. [PLATANIOTIS/VENETSANOPOULOS 00] Plataniotis, K. N.; Venetsanopoulos, A. N.: *Color Image Processing and Applications*. Springer; Berlin etc. 2000

-
27. [RICHTER 66] Richter, H.: *Wahrscheinlichkeitstheorie*. Springer; Berlin - Heidelberg - New York 1966 (Grundlehren 86), 2nd ed.
 28. [SCHERZER/GRASMAIR/GROSSAUER/HALTMEIER/LENZEN 09] Scherzer, O.; Grasmair, M.; Grossauer, H.; Haltmeier, M.; Lenzen, F.: *Variational Methods in Imaging*. Springer; New York etc. 2009
 29. [WÄCHTER/BIEGLER 06] Wächter, A.; Biegler, L. T.: *On the implementation of an interior-point filter line-search algorithm for large-scale nonlinear programming*. Math. Program. Ser. A **106** (2006), 25 – 57
 30. [WAGNER 10] Wagner, M.: *Elastic image registration in presence of polyconvex constraints*. Karl-Franzens-Universität Graz, SFB-Report No. 2010-033. Status: accepted (Proceedings of the International Workshop on Optimal Control in Image Processing, Heidelberg, Germany, May 31 - June 1, 2010)
 31. [WAGNER 12] Wagner, M.: *A direct method for the solution of an optimal control problem arising from image registration*. Numerical Algebra, Control and Optimization **2** (2012), 487 – 510
 32. [ZITOVÁ/FLUSSER 03] Zitová, B.; Flusser, J.: *Image registration methods: a survey*. Image and Vision Computing **21** (2003), 977 – 1000

Last modification: 18.12.2012 / 11.04.2013

Author's addresses. Angel Angelov: Otto-Hahn-Str. 15, D-30880 Laatzen, Germany.

e-mail: angelov.angel@gmx.de

Marcus Wagner: University of Leipzig, Department of Mathematics, P. O. B. 10 09 20, D-04009 Leipzig, Germany.

Homepage / e-mail: www.thecityto come.de / marcus.wagner@math.uni-leipzig.de